Locomotion over a Washboard

by

Yi Sui

B.A., University of California, Berkeley, 2012

A THESIS SUBMITTED IN PARTIAL FULFILLMENT OF
THE REQUIREMENTS FOR THE DEGREE OF

MASTER OF SCIENCE

in

The Faculty of Graduate and Postdoctoral Studies

(Mathematics)

THE UNIVERSITY OF BRITISH COLUMBIA

(Vancouver)

January 2015

Abstract

The purpose of this thesis is to study the problem when a microorganism swims very close to a shaped boundary. In this problem, we model the swimmer to be a two-dimensional, infinite periodic waving sheet. For simplicity, we only consider the case where the fluid between the swimmer and the washboard is Newtonian and incompressible. We assume that the swimmer propagates waves along its body and propels itself in the opposite direction.

We consider two cases in our swimming sheet problem and the lubrication approximation is applied for both cases. In the first case, the swimmer has a known fixed shape. Various values of wavenumber, amplitude of the restoring force and amplitude of the topography were considered. We found the instantaneous swimming speed behaved quite differently as the wavenumber was varied. The direction of the swimmer was also found to depend on the amplitude of the restoring force. We also found some impact of the topographic amplitude on the relationship between average swimming speed and the wavenumber. We extended the cosine wave shaped washboard to be a more general shape and observed how it affected the swimming behaviour.

In the second case, the swimmer is assumed to be elastic. We were interested to see how different values of wavenumber, stiffness and amplitude of the restoring force could change the swimming behaviour. With normalized stiffness and wavenumber, we found the swimmer remained in a periodic state with small forcing amplitude. While the swimmer reached a steady state with unit swimming speed for high forcing amplitude. However, for other values of stiffness and wavenumber, we found the swimmer's swimming behaviour was very different.

Preface

This thesis is original, unpublished, independent work by the author, Y. Sui under the supervision of Dr. N. J. Balmforth.

Table of Contents

List of Figures

Acknowledgements

I would like to thank my supervisor, Dr. Neil Balmforth, for all his generous support, help, and patience through the completion of this thesis work. Thanks to Neil for introducing me to the field of fluid dynamics. I would like to thank Dr. Daniel Coombs for taking time reading through my thesis.

I would like also thank other professors at UBC whom I have taken courses from. I also owe thanks to all my friends and staff members at the IAM and UBC math department. They have been very supportive for the past two years. I will never forget these two wonderful years at UBC.

Finally, special thanks to my families for their endless love, support and encouragement.

Dedication

To my parents for always being there for me.

Chapter 1

Introduction

If we look at a spermatozoon and an eel-like fish swimming in the water, we will see both of them swimming with wave-like movements, where they both produce a wave that travels backwards along the body, pushing the water backwards and the entire body forwards [2]. One might ask, though the phenomena of a spermatozoon and eel-like fish swimming look the same, are there actually different underlying physical mechanisms underlying what we have seen? The answer is yes and the difference can be easily explained using the quantity called the Reynolds number. Normally, the Reynolds number for a swimming fish is on the order of 10^2, while for tiny organism like spermatozoon it goes down to about 10^{-3} or less. When the eel-like fish swims in the water, its wave-like movements give rise to circulations around the body and then it driven forwards by the inertial forces set up in the surrounding fluid. However, when a spermatozoon swims in the water, due to the small value of the Reynolds number, the force due to viscosity is much greater than the one due to inertia. Here comes the question: how can a body propel itself when inertial forces are small compared to the forces due to viscosity? [30, 33, 35, 42, 43].

The study of the physics of locomotion at low Reynolds number has a long history. Since the 1930s, the swimming of various microorganisms like *E. coli*, paramecium, and spermatoza has been studied by lots of researchers [32]. Spermatozoon motility has attracted the most attention, mainly due to the fact that spermatozoon swimming is simpler to model and due to the biological importance of spermatozoa. Motile bacteria commonly have many flagella distributed in various ways over the cell, and their different flagella may rotate or corkscrew together as a flagellar bundle. This is essentially three dimensional and so it will be very hard to find a simple model to

represent the swimming of these bacteria. However, spermatozoa have only two parts: a head and a long flagellum. The flagellum beats, producing waves that propel the body through the fluid. Due to this simple simple structure, it is possible to model the swimming of spermatozoon using a simple two-dimensional model introduced by G. I. Taylor [1, 11, 35, 42]. On the other hand, the huge number of unsolved problems in the locomotion of mammalian sperm also motivate people to continue to model the movement of spermatozoa. The goal of the research is ultimately to help physicians find the cure for significant health problems such as infertility and unintended pregnancies [26, 39].

Significant contributions to the field of swimming microorganism have been made by many scientists, including G. I. Taylor, A. J. Reynolds, J. R. Blake, J. Gray, G. J. Hancock and D. F. Katz [4, 6, 14, 22, 25, 36, 42, 43]. Even though some of this work is over 60 years old, their work still motivates people to continue research on the field of locomotion at low Reynolds number.

The purpose of this thesis is to extend work done by G. I. Taylor [42, 43] and D. F. Katz [25], by looking at the problem of a microorganism swimming close to a washboard in a Newtonian fluid. We will assume that the swimmer propagates waves along its body and propels itself in the opposite direction. We consider the swimmer to be a two-dimensional and infinitely periodic thin sheet. Instead of a single plane wall presented close to the swimmer which has been looked at by Katz [25], we will examine a more complicated geometry where there is a washboard present. This geometry allows us to model the natural situation where a microorganism needs to swim over a more geometrically complex environment than a plane wall [34]. In this thesis, we consider two cases of the swimming problem. In the first case, we assume the swimmer has a fixed shape given by a simple sine wave. In the second case, we assume the shape of the swimmer is unknown. However, we will suppose there is a force distributed along the body of the swimmer. This force will be obtained from a simple elastic beam theory. In both these two cases, we assume the lubrication approximation. We examine different values of wavenumber of the swimmer and amplitude of the force driving the

locomotion of the swimmer to see how it affects the swimming behaviour. In particular, for the case of the fixed shape swimmer, we looked at different shapes of the washboard.

In this chapter, we will first do a literature review to outline some significant previous work in the field of swimming microorganisms. We will then set up the main problem we will consider in this thesis with an explanation of all the necessary assumptions we have used. Finally, we will outline the structure of this thesis.

1.1 Literature Review

The study of locomotion of animals has a very long history, and there are lots of publications on this topic. Among them, J. Gray and his colleagues made particularly significant contributions to the topic of locomotion of fish in a series of articles published on the *Journal of Experimental Biology* during the 1930s [2, 16–21, 33]. In this thesis, instead of looking at the swimming fish, we would like to particularly study the swimming of microorganisms at low Reynolds number. Since 1950s, various researchers have paid lots of attention to swimming microorganisms, and in particular they were interested in analyzing how fast the organisms could swim. Here, we will outline some literature covering the topic of swimming microorganisms.

In 1952, G. I. Taylor published a paper analyzing the swimming of microorganisms with an asymptotic approach [42]. Taylor assumed that the spermatozoon swam in the viscous fluid as a two-dimensional, infinite, inextensible thin sheet. The amplitude of the swimming wave was taken to be small. The waving surface was represented by a simple sine curve

$$y_0 = b\sin(kx - \sigma t). \tag{1.1}$$

The velocity of the wave is σ/k, the wave length is $2\pi/k = \lambda$, and t represents time. The amplitude b was assumed to be small compared to λ and the waving sheet moved in the positive x direction. Solving the two dimensional Navier-Stocks equations of Newtonian fluids (with inertia term neglected),

Taylor found that the wave in the sheet could not propel it through the fluid at the first order in b. However, when he carried on the calculation to the second order, he found a nonzero swimming speed. In dimensional units, the swimming speed V he found was

$$\frac{Vk}{\sigma} = \frac{1}{2}b^2k^2\left(1 - \frac{19}{16}b^2k^2\right). \tag{1.2}$$

This formula shows that the leading order of swimming speed is proportional to the amplitude of the swimming wave squared. In the paper, he also calculated the mean value of the dissipation of energy W, finding

$$W = 2b^2\sigma^2k\mu\overline{\cos^2(kx - \sigma t)} = b^2\sigma^2k\mu. \tag{1.3}$$

In addition to these, Taylor also examined the case where there was a viscous fluid on both sides of the sheet. He found that the swimming speed V was as the same rate as for the situation where there was fluid only on one side. However, the rate of dissipation of energy increased to be $2W$ instead of W. In addition to this paper, Taylor had a later paper in 1952 which assumed the tail of spermatozoon was a flexible cylindrical shape instead of a thin sheet. He first considered the case where the swimmer propagated waves backwards along the tail to achieve a motion. He found, in this case, the swimming velocity was proportional to the square of the ratio of the amplitude of the wave to the wave length. He then considered a second case where the tail propagated a wave of spiral form and found that in this situation the body was propelled twice as fast as the case where the wave was propagated along the tail [43].

In 1965, A. J. Reynolds published a paper with an extension of the previous work of Taylor [36]. In this paper, same as Taylor's paper, he assumed the swimming object was a two dimensional waving sheet with the profile $y = b\sin(kx + \sigma t)$, the amplitude of the wave was small, and the method of asymptotic analysis was applied. In this paper, he generalized Taylor's study in three respects. First, instead of looking at low Reynolds number object where inertia got neglected, Reynolds assumed there is an finite inertia

of the perturbed fluid. Solving the corresponding Navier-Stocks equations with appropriate boundary conditions applied, he found the second-order propulsive velocity to be

$$\frac{V}{U} = \frac{1}{4}\alpha^2 \left[\frac{\beta - \cos\phi}{\cos\phi - 1/\beta} - 1 \right], \tag{1.4}$$

where V is the propulsive speed, U is the wave velocity and α is bk. s is defined as $U/\nu k$, where ν is the viscosity, $\beta = (1 + s^2)^{1/4}$ and $\cos\phi = [(1 + \beta^2)/2\beta^2]^{1/2}$. When there was a large viscosity, he saw

$$\frac{V}{U} \to \frac{1}{2}\alpha^2, \tag{1.5}$$

which matched with what Taylor had found for low Reynolds number swimmers. Second, he looked at the case where the waving sheet was extensible with the inertia of the fluids neglected. The velocity solution he found matched with what Taylor had found when the extensibility parameter δ approaches zero. Finally, he considered the case when the swimmer swam near a solid wall. When the waving sheet swims in the centre of a channel of width $2h$, the swimming velocity satisfies

$$\frac{V}{U} = \frac{1}{2}\alpha^2 \left[\frac{\sinh^2(kh) + k^2h^2}{\sinh^2(kh) - k^2h^2} \right]. \tag{1.6}$$

While, when the waving sheet is in a channel at a distance $h1$ from one wall and $h2$ from the other,

$$\frac{V}{U} = \frac{1}{2}\alpha^2 \left[-(1 + d_1 + d_2) + \frac{(h_1 - h_2)(d_1 - d_2)}{(h_1 + h_2)} \right], \tag{1.7}$$

where $d = \sinh^2(kh)/[\sinh^2(kh) - k^2h^2]$.

Another great extension of Taylor's two dimensional waving sheet problem was done by D. F. Katz. In [25], Katz solved the swimming sheet problem using both biharmonic and lubrication analysis with valid assumptions. He assumed the sheet swims inside of a channel, where one of the walls was defined as $y = h_1$ and another one was $y = -h_2$. The sheet propa-

gated a wave along its body in the negative x direction with speed c, which propelled the sheet in the positive x direction with velocity V. He set the point on the sheet surface, (x_0, y_0), to be

$$x_0 = x_m + a\cos k[x_m + (c - V)t] + d\sin k[x_m + (c - V)t], \tag{1.8}$$

$$y_0 = b\sin k[x_m + (c - V)t], \tag{1.9}$$

where $(x_m, 0)$ is the mean position of (x_0, y_0). Notice this set-up is more general than what G. I. Taylor did in [42]. By assuming that the amplitude of the wave was small, Katz applied biharmonic analysis and found that the leading order of swimming speed is proportional to the amplitude of the swimming sheet squared, which matched with what had been found by Taylor. Thus, the presence of walls doesn't alter the leading order swimming speed. Furthermore, he considered the case when a sheet swam in a narrow channel. Next, instead of biharmonic analysis, lubrication-theory analysis was applied. He found the leading order of swimming speed in the dimensional variables as

$$\frac{V_0}{c} = \frac{3}{(h/b)^2 + 2}, \tag{1.10}$$

where h measures the distance between two walls. It indicated that to the lowest order, velocity of propulsion is bounded by the wave speed. Beyond doing the asymptotic analysis of the two dimensional swimming sheet problem, Katz also did lots of experiments to look at how spermatozoa swim in the real world [27–29].

In addition to the flagellate microorganisms, like spermatozoa, we have been looking at, there is another common type of microorganism called a ciliate, which consists of a body that is covered by a great number of hair-like organelles [30]. Many researchers have paid lots of attention to analyzing the swimming of ciliates. However, due to the more complicated structure, the ciliates can't be simply modelled by a two dimensional model. Instead, a three dimensional model will be needed. In early 1970s, J. R. Blake published a series of articles using a spherical envelope model. In the

three dimensional spherical envelope model, he assumed the organism was spherical. There was a surface covering the ends of the numerous undulating cilia over the surface of the organism called the "envelope". The no-slip condition was applied at the surface of the waving envelope. Blake first considered a finite spherical envelope approach and found the mean velocity $\bar{U}$ was proportional to $a\sigma$, where a was the radius of the organism and σ was the angular frequency of movement of the cilium. By taking a finite valued N in the Taylor series expansion with a reasonable a and σ value plugged in, he found this model agreed with velocities experienced in nature [6]. Blake then considered an infinite spherical model and found that as the radius of the organism increased, the result of the infinite spherical model tended to that for the waving sheet. And the velocity of the propulsion for the infinite model was over twice that obtained for the finite spherical model [4, 5]. Later in 1972, based on previous work, Blake wrote a couple of articles considering an alternative cilia sublayer method to look at the velocity of ciliary locomotion [7–9].

The swimming problem of microorganisms is not only studied analytically, but also studied numerically. A couple of papers written by L. J. Fauci and her team in the 1990s particularly looked at the swimming of spermatozoon numerically [13, 15]. In both of the articles, Fauci studied the fluid dynamics of sperm motility using the immersed boundary method. In [15], she modelled when spermatozoon swam near a rigid or elastic wall and also when both single and several organisms were present. After comparing the numerical results with analytical results, she found her results matched with what Katz had found [25]. In the Early 2000s, she and M. M. Hopkins did further numerical analysis of the swimming of geotactic, gyrotactic and chemotactic microorganisms [23].

More recent publications of swimming microorganisms have examined viscoelastic fluids instead of simple Newtonian fluids. It makes more physical sense to look at complex fluids because in nature, the biological environment microorganisms experience often features complex fluids due to the presence of biopolymers [32, 45]. In [31], E. Lauga revisited Taylor's swimming sheet problem where the fluid was non-Newtonain. He considered the cases where

the Deborah number of the fluid was moderate or high and where the propagating wave included normal and tangential motion. He found that in all cases the velocities of the swimming sheet were smaller than for motion in a Newtonian fluid. Further experimental observations done by X. N. Shen and P. E. Arratia [37] have supported the theoretical predictions described in [31]. In addition to these, Balmforth *et al.* wrote a paper particularly looking at the influence of shear thinning, shear thickening and yield stress fluids when microorganisms swim very close to a solid boundary [3].

In a recent paper, Majmudar *et al.* pointed out that in nature swimming microorganisms often need make their way through a fluid with obstacles. They did both experiments and numerical analysis to see how microorganisms successfully navigated around the obstacles and how obstacles changed the swimming path and speed of the microorganism [34]. Inspired by their work and the work done by Balmforth *et al.* [3, 34], in this thesis, we consider the situation when the microorganism swims near a washboard. We model the swimmer as a two dimensional, infinite periodic and inextensible thin sheet. To be simple, we assume the fluid between the swimmer and the wavy wall is Newtonian and incompressible. In this thesis, we will consider two cases: when the swimmer has a fixed shape and when the swimmer is an elastic swimmer. We are interested to see how different values of wavenumber, wave amplitude, and stiffness change the swimming behaviour.

1.2 Our Main Problem

Now we know why we are interested in this problem and what others have done to study locomotion at low Reynolds number, we are in a good position to set up our main problem mathematically.

In our problem, we consider the swimmer to be two-dimensional and infinitely periodic, and assume that it swims close to a washboard. For simplicity, we would like to consider the fluid between the swimmer and the washboard as Newtonian and incompressible. We assume that the swimmer propagates waves along its body and propels itself in the opposite direction. We call the swimming speed in time t, $U(t)$, and the wave speed C. It is

assumed in the problem that the swimmer propagates waves along its body in the negative x-direction, so propelling itself to the positive x-direction with a velocity of $U(t)$. Let the shape of the swimmer be $y = Y(x,t)$ which is centred at $y = 0$, and the washboard is fixed at the position $y = h(x)$. The distance between the swimmer and the washboard will be called $d(x,t) = Y(x,t) - h(x)$.

The problem satisfies the two-dimensional Navier-Stokes equations and the continuity equation:

$$\rho \left(\frac{\partial \mathbf{u}}{\partial t} + \mathbf{u} \cdot \nabla \mathbf{u} \right) = -\nabla p + \nabla \cdot \tau + \mathbf{F}, \tag{1.11}$$

$$\nabla \cdot \mathbf{u} = 0. \tag{1.12}$$

Here ρ is the fluid density, $\mathbf{u} = (u, v)$ is the velocity field, p is the pressure within the fluid, τ is the deviatoric component of the stress tensor and $\mathbf{F}$ represents body forces acting on the fluid.

In the fixed reference frame, the velocity field $\mathbf{u} = (u, v)$ along $y = Y(x,t)$ satisfies

$$u(x, Y) = U(t), \tag{1.13}$$

$$v(x, Y) = Y_t + UY_x. \tag{1.14}$$

When $y = h(x)$, the no-slip boundary condition gives

$$u(x, h) = 0, \tag{1.15}$$

$$v(x, h) = 0. \tag{1.16}$$

Hence, full geometry of the problem looks like the following:

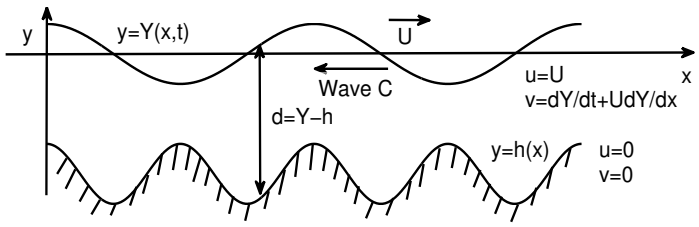

Figure 1.1: A sketch of the geometry of the problem.

Along with these equations, based on the physical situation we are looking at, we will make several assumptions to simplify the problem a little bit and help us to solve the system.

Because we look at the behaviour of micro-organisms, low Reynolds number will be considered due to great physical interests. That is,

$$0 < Re \ll 1.$$

In this sense, the inertial terms on the left hand of the Navier-Stokes equations can be neglected. It will be also assumed that there is no external force acting in the problem. i.e.

$$\mathbf{F} = 0.$$

Since we will only deal with Newtonian fluid, the shear stress term, $\nabla \cdot \tau$, can be simplified to $\mu \nabla^2 \mathbf{u}$, where μ is the viscosity of the fluid. It will also be assumed that the amplitude of the propagating wave is small compared to its wavelength. It makes physical sense because it has been found that freshly ejaculated sperm tend to swim with low amplitude and symmetric flagellar beats [40]. Meanwhile, it is assumed that the problem is periodic. In particular, we will look at the periodicity of pressure p in x. Moreover, the equation of motion of the swimmer gives that

$$\text{mass per length} \times \text{acceleration} = \text{net force}.$$

Because we are looking at the situation having no inertia, the left hand side of the equation of the motion is equal to zero and therefore the net force on the swimmer is zero.

Note the set-up of the problem described above will apply to all chapters in this thesis.

1.3 Thesis Outline

In Chapter Two, we will look at the problem of a fixed shape swimming sheet swimming near a washboard. The lubrication theory approximation is applied. First, we consider the case when the washboard has a simple cosine shape. Various values of wavenumber, amplitude of the resorting force and amplitude of the topography are considered. We will look at the instantaneous swimming speed and the average swimming speed of the swimmer. Here, a simple case when the wavenumber is equal to one will be studied analytically, while other cases will be done numerically. Later, we will also look at the case when the washboard has a more general shape.

In Chapter Three, we will look at the problem of an elastic swimming sheet swimming near a sinusoidal washboard. The lubrication theory approximation is applied. Various values of wave amplitude and wavenumber are considered. We also look at the effects of stiffness. Here, all the work will be done numerically.

In Chapter Four, a summary of what we have found will be included with a mention of the future work could be done.

Chapter 2

Fixed Shape Swimmer with Lubrication Theory Analysis

We will apply lubrication theory analysis through out this chapter, similar to the work shown in [25] by Katz. In order to apply lubrication theory here, we will assume the mean distance between the swimmer and the wavy wall, $\bar{d}$, compared with the wavelength of the swimmer, k, is very small. In Katz's paper, he assumed the swimmer had a fixed shape which is defined by a sine wave. Carrying on Katz's analysis, we will focus on the situation where the swimmer has a fixed shape in this chapter.

In the chapter, we will look at cases with a small amplitude or high amplitude force driving the locomotion of the swimmer. We will also look at various values of wavenumber and various values of the amplitude of the topography to see how they change the swimming behaviour.

2.1 Lubrication Theory Model

Recall that in our problem, there is a swimmer swimming near the washboard with Newtonian fluid in between. We begin by considering the problem in the fixed reference frame.

In order to apply the lubrication approximation, we have assumed the mean distance between the swimmer and the wavy wall is very small compared to the wavelength of the swimmer, i.e.

$$0 < \bar{d}k = \epsilon \ll 1. \tag{2.1}$$

With the assumptions mentioned in Chapter One, our problem satisfies

the conservation of momentum and mass equations as

$$\rho\left(\frac{\partial \mathbf{u}}{\partial t} + \mathbf{u}\cdot\nabla\mathbf{u}\right) = -\nabla p + \mu\nabla^2\mathbf{u}, \tag{2.2}$$

$$\nabla\cdot\mathbf{u} = 0. \tag{2.3}$$

The boundary conditions on the lower surface of the locomotor, $y = Y(x,t)$, are

$$u(x,Y) = U(t), \tag{2.4}$$

$$v(x,Y) = Y_t + UY_x. \tag{2.5}$$

The boundary conditions on the stationary washboard, $y = h(x)$, are

$$u(x,h) = 0, \tag{2.6}$$

$$v(x,h) = 0. \tag{2.7}$$

The normal force balance on the upper surface of the fluids dictates that

$$p = DY_{xxxx} - f, \tag{2.8}$$

where D is a parameter measuring the stiffness of the swimmer, p is the pressure, Y is the shape of the swimmer, and f is the applied restoring force, which drives the locomotion of the swimmer. We define the restoring force, f, as

$$f(x,t) = A\cos k\left(x - \int_0^t U(\hat{t})\ d\hat{t} + Ct\right), \tag{2.9}$$

where A denotes the force strength. We assume the restoring force f produces a propagating wave along the swimmer to the negative x direction with a speed of C. Note that equation (2.8) could be used to determine the shape of the swimmer Y.

Moreover, we assume the stationary washboard looks like

$$h(x) = b\cos Kx - \bar{d} \tag{2.10}$$

where b measures the amplitude of the washboard.

Now we can non-dimensionalize the problem using the following non-dimensional variables:

$$\begin{aligned}
\tilde{x} &= kx, \qquad \tilde{y} = y/\bar{d},\\
\tilde{t} &= kCt, \qquad \tilde{u} = u/C,\\
\tilde{v} &= v/v_c \;\Rightarrow v_c = \epsilon C,\\
\tilde{p} &= p/p_c, \;\Rightarrow p_c = \frac{C\mu}{k\bar{d}^2}.
\end{aligned}$$

Upon substituting these non-dimensional variables, the x-component of the equation of conservation of momentum becomes:

$$\begin{aligned}
\rho\left(C^2k\frac{\partial\tilde{u}}{\partial\tilde{t}} + C^2k\tilde{u}\frac{\partial\tilde{u}}{\partial\tilde{x}} + \frac{\epsilon C^2}{\bar{d}}\tilde{v}\frac{\partial\tilde{u}}{\partial\tilde{y}}\right) &= -p_ck\frac{\partial\tilde{p}}{\partial\tilde{x}} + C\mu k^2\frac{\partial^2\tilde{u}}{\partial\tilde{x}^2} + \frac{C\mu}{\bar{d}^2}\frac{\partial^2\tilde{u}}{\partial\tilde{y}^2}\\
\Rightarrow Re\;\epsilon^2\left(\frac{\partial\tilde{u}}{\partial\tilde{t}} + \tilde{u}\frac{\partial\tilde{u}}{\partial\tilde{x}} + \tilde{v}\frac{\partial\tilde{u}}{\partial\tilde{y}}\right) &= -\frac{\partial\tilde{p}}{\partial\tilde{x}} + \epsilon^2\frac{\partial^2\tilde{u}}{\partial\tilde{x}} + \frac{\partial^2\tilde{u}}{\partial\tilde{y}^2},
\end{aligned}$$

where Re is the Reynolds number defined as

$$Re = \frac{\rho C}{\mu k}.$$

As $Re \to 0$ and $\epsilon \to 0$, this gives

$$\bar{p}_{\tilde{x}} = \tilde{u}_{\tilde{y}\tilde{y}}. \tag{2.11}$$

The y-component becomes

$$\rho\left(\epsilon C^2 k\frac{\partial\tilde{v}}{\partial\tilde{t}}+\epsilon C^2 k\tilde{u}\frac{\partial\tilde{v}}{\partial\tilde{x}}+\frac{\epsilon^2C^2}{\bar{d}}\tilde{v}\frac{\partial\tilde{v}}{\partial\tilde{y}}\right)=-\frac{P_c}{\bar{d}}\frac{\partial\tilde{p}}{\partial\tilde{y}}+\mu\left(\epsilon k^2C\frac{\partial^2\tilde{v}}{\partial\tilde{x}^2}+\frac{\epsilon C}{\bar{d}^2}\frac{\partial^2\tilde{v}}{\partial\tilde{y}^2}\right)$$
$$\Rightarrow Re\ \epsilon^4\left(\frac{\partial\tilde{v}}{\partial\tilde{t}}+\tilde{u}\frac{\partial\tilde{v}}{\partial\tilde{x}}+\tilde{v}\frac{\partial\tilde{v}}{\partial\tilde{y}}\right)=-\frac{\partial\tilde{p}}{\partial\tilde{y}}+\epsilon^4\frac{\partial^2\tilde{v}}{\partial\tilde{x}^2}+\epsilon^2\frac{\partial^2\tilde{v}}{\partial\tilde{y}^2}$$

As $Re\to 0$ and $\epsilon\to 0$, this gives

$$\tilde{p}_{\tilde{y}}=0. \tag{2.12}$$

The continuity equation is

$$Ck\frac{\partial\tilde{u}}{\partial\tilde{x}}+\frac{\epsilon C}{\bar{d}}\frac{\partial\tilde{v}}{\partial\tilde{y}}=0$$
$$\Rightarrow \tilde{u}_{\tilde{x}}+\tilde{v}_{\tilde{y}}=0. \tag{2.13}$$

Moreover, the dimensionless equation of topography will be

$$h(x)=b\cos Kx-\bar{d}\Rightarrow\tilde{h}(\tilde{x})=\tilde{b}\cos(\kappa\tilde{x})-1, \tag{2.14}$$

where $\kappa=K/k$ is called the wavenumber and it is selected to be a rational number in order to allow for a periodic geometry.
The dimensionless form of the restoring force f is

$$f(x,t)=A\cos k\left(x-\int_0^t U(\hat{t})\ d\hat{t}+Ct\right)$$
$$\Rightarrow f(\tilde{x},\tilde{t})=\tilde{A}\cos\left(\tilde{x}-\int_0^{\tilde{t}}\tilde{U}(\hat{\tilde{t}})\ d\hat{\tilde{t}}+\tilde{t}\right). \tag{2.15}$$

Thus, we could get the dimensionless form of (2.8) by taking the non-dimensional $\tilde{A}$ and $\tilde{D}$ as

$$\tilde{D}=\frac{\bar{d}^3k^5}{c\mu}D,\qquad \tilde{A}=\frac{C\mu}{k\bar{d}^2}A.$$

Note: From now on, everything will be dimensionless. To make things

simple, we will drop the tilde notation.

From (2.12), we can see that the pressure p is independent of y, i.e. $p(x,t)$. We can integrate (2.11) twice, it gives:

$$u(x,y) = \frac{p_x}{2}y^2 + Ey + F.$$

Since $u(x,h) = 0$ and $u(x,Y) = U$,

$$\begin{aligned} \Rightarrow E &= \frac{U}{Y-h} - \frac{p_x}{2}(Y+h), \\ F &= -\frac{p_x h^2}{2} + \left(\frac{p_x}{2}(Y+h) - \frac{U}{Y-h}\right)h = \frac{p_x Y h}{2} - \frac{Uh}{Y-h}. \end{aligned}$$

It implies that

$$\begin{aligned} u(x,y) &= \frac{p_x y^2}{2} + \left(\frac{U}{Y-h} - \frac{p_x}{2}(Y+h)\right)y + \frac{p_x Y h}{2} - \frac{Uh}{Y-h} \\ &= \frac{1}{2}p_x(y-Y)(y-h) + \frac{U}{Y-h}(y-h). \end{aligned} \tag{2.16}$$

From (2.13), we know that

$$u_x + v_y = 0 \Rightarrow v_y = -u_x.$$

Integrating in y from h to Y, it gives that

$$\int_h^Y v_y \, dy = -\int_h^Y u_x \, dy, \tag{2.17}$$

Applying Leibniz integral rule gives

$$\frac{d}{dx}\left(\int_h^Y u \, dy\right) = \int_h^Y u_x \, dy + u(Y)Y_x - u(h)h' = \int_h^Y u_x \, dy + UY_x,$$

since $u = 0$ on $y = h$ and $u = U$ on $y = Y$. Thus, (2.17) can be rewritten as

$$\begin{aligned}\int_h^Y v_y \, dy &= UY_x - \frac{d}{dx}\left(\int_h^Y u \, dy\right) \\ \Rightarrow v(Y) &= UY_x - \frac{d}{dx}\left(\int_h^Y u \, dy\right),\end{aligned}$$

because $v = 0$ on $y = h$. Recall that the vertical velocity v on $Y(x,t)$ satisfies $v(Y) = Y_t + UY_x$. It follows that

$$Y_t = -\frac{d}{dx}\left(\int_h^Y u \, dy\right).$$

Plugging the velocity equation of u found in (2.16) into above equation gives

$$\begin{aligned}Y_t &= -\frac{d}{dx}\left[\int_h^Y \left(\frac{1}{2}\, p_x(y-Y)(y-h) + \frac{U}{Y-h}(y-h)\right) dy\right] \\ &= \frac{d}{dx}\left(\frac{p_x}{12}(Y-h)^3 - \frac{U}{2}(Y-h)\right),\end{aligned} \tag{2.18}$$

in the fixed lab reference frame.

We can change every thing into the moving reference frame, $(\check{x}, t)$, by defining

$$x = \check{x} + \int_0^t U(\hat{t}) \, d\hat{t} \quad \Rightarrow \frac{dx}{dt} = \frac{d\check{x}}{dt} + U.$$

Now (2.18) could be rewritten using the moving reference frame as

$$\begin{aligned}Y_t &= UY_{\check{x}} + \frac{d}{d\check{x}}\left(\frac{p_{\check{x}}}{12}(Y-h)^3 - \frac{U}{2}(Y-h)\right) \\ &= \frac{d}{d\check{x}}\left(\frac{p_{\check{x}}}{12}(Y-h)^3 + \frac{U}{2}(Y-h)\right).\end{aligned} \tag{2.19}$$

Furthermore, we can change (2.19) into the wave reference frame, (ξ, t), as

$$\begin{aligned} Y_t &= UY_{\check{x}} + \frac{d}{dx}\left(\frac{p_x}{12}(Y-h)^3 - \frac{U}{2}(Y-h)\right) \\ \Rightarrow (1-U)Y_\xi &= \frac{d}{d\xi}\left(\frac{p_\xi}{12}(Y-h)^3 - \frac{U}{2}(Y-h)\right), \end{aligned} \tag{2.20}$$

where the horizontal spatial coordinate in the moving reference frame is defined as

$$\xi = \check{x} + t = x - \int_0^t U(\hat{t})\ d\hat{t} + t.$$

Integrating (2.20) over ξ leaves

$$\begin{aligned} Q(t) + (1-U)Y &= \frac{p_\xi}{12}(Y-h)^3 - \frac{U}{2}(Y-h) \\ \Rightarrow Q(t) &= \frac{p_\xi}{12}(Y-h)^3 - \frac{U}{2}(Y+h) - Y, \end{aligned} \tag{2.21}$$

where $Q(t)$ is the flux in the wave frame.

2.1.1 Periodicity in Pressure Condition

A key assumption mentioned in Chapter One is that the periodic condition of pressure p in x.

Rearranging (2.21) we can get a equation of p_ξ in terms of the flux, $Q(t)$, as

$$p_\xi = \frac{12}{(Y-h)^3}\left(Q(t) + Y - \frac{U}{2}(Y+h)\right).$$

Notice in the fixed reference frame, it is

$$p_x = \frac{12}{(Y-h)^3}\left(Q(t) + Y - \frac{U}{2}(Y+h)\right). \tag{2.22}$$

Since pressure p is periodic in x, we will have $\langle p_x \rangle = 0$. Here,

$$\langle \cdots \rangle = \frac{1}{L} \int_0^L (\cdots)\, dx,$$

where L denotes the length of individual periodic section of the swimmer and is set to be $2\pi k$. It indicates that the periodic sections of the swimmer contains k wavelengths of the forcing and K wavelength of the topography in length L.

2.1.2 Zero Net Force Condition

The traction on the lower surface of the swimmer drives its locomotion, which gives an additional dynamical condition on the swimmer. Recall, in Chapter One, we have stated that the equation of motion of the swimmer is

$$\text{mass per unit length} \times \text{acceleration} = \text{net force}.$$

We know the force on the fluid surface due to the fluid stress at $y = Y$ is equal to the force on swimmer due to the fluid, and the stress tensor of the fluids in the dimensional form looks like

$$\sigma \equiv \begin{pmatrix} -p + 2\mu u_x & \mu\,(u_y + v_x) \\ \mu\,(u_y + v_x) & -p + 2\mu v_y \end{pmatrix}.$$

In the lubrication limit, it can be simplified to

$$\sigma \equiv \begin{pmatrix} -p & \mu u_y \\ \mu u_y & -p \end{pmatrix}.$$

The outwards unit normal vector, $\mathbf{n}$, along the swimmer Y is

$$\mathbf{n} = \frac{(-Y_x, 1)}{\sqrt{1 + Y_x^2}},$$
$$\Rightarrow \sigma \cdot \mathbf{n} = \begin{pmatrix} -p & \mu u_y \\ \mu u_y & -p \end{pmatrix} \cdot \begin{pmatrix} -Y_x \\ 1 \end{pmatrix} \Big/ \sqrt{1 + Y_x^2}\,.$$

According to the Newton's Second Law, the acceleration of the swimmer and the net force on the swimmer in the x direction satisfy

$$M\dot{U} = -\langle p(x,t)Y_x + \mu u_y(x,Y,t)\rangle, \tag{2.23}$$

where M indicates the effective inertia of the swimmer and $\langle\cdots\rangle$ denotes the x-average defined same as before. With periodic condition of p in x and applying the Leibniz integral rule, we will have

$$M\dot{U} = -\langle \mu u_y(x,Y,t) - p_x(x,t)Y\rangle. \tag{2.24}$$

Since we are looking at the problem for a micro-organism, the problem is considered to be inertialess, i.e. $M \to 0$. Then, (2.23) is reduced to be an integral constraint

$$0 = \langle p(x,t)Y_x + \mu u_y(x,Y,t)\rangle.$$

Non-dimensionalizing the above equation using the same non-dimensional variables defined in the previous section, we get a dimensionless form integral constraint as

$$0 = \langle p(x,t)Y_x + u_y(x,Y,t)\rangle. \tag{2.25}$$

2.2 Swimming with a Fixed Shape

In this chapter, we focus on the case when the swimmer has a fixed shape as discussed in paper [25] written by Katz, i.e. the swimmer has an infinite stiffness. In this situation, from (2.8), we get the following relation:

$$p \ll DY_{xxxx} - f \;\Rightarrow 0 \approx DY_{xxxx} - f.$$

Since $f(x,t) = A\cos\left(x - \int_0^t U(\hat{t})\ d\hat{t} + t\right)$, the above relation can be rewritten as

$$Y_{xxxx} = \frac{A}{D}\cos\left(x - \int_0^t U(\hat{t})\ d\hat{t} + t\right). \tag{2.26}$$

Integrating (2.26) four times and applying the corresponding periodic boundary conditions, i.e. Y is periodic up to and including its third derivatives, gives

$$Y = a\cos\left(x - \int_0^t U(\hat{t})\ d\hat{t} + t\right) = a\cos\xi, \tag{2.27}$$

where $a = A/D$ and ξ is the horizontal spatial coordinate in the wave reference frame.

Moreover, we can plug (2.22) into the periodic condition $\langle p_x \rangle = 0$, and get

$$\begin{aligned} &\left\langle \frac{12}{(Y-h)^3}\left(Q(t) + Y - \frac{U}{2}(Y+h)\right)\right\rangle = 0 \\ &\Rightarrow I_3^0 Q = \left(I_3^1 - \frac{1}{2}I_2^0\right)U - I_3^1, \end{aligned} \tag{2.28}$$

where

$$I_n^m \equiv \left\langle \frac{Y^m}{(Y-h)^n}\right\rangle.$$

We plug in (2.16) and (2.22) into (2.25) and get

$$\left(\frac{1}{2}I_2^0 - I_3^1\right)Q + \left(I_3^2 - I_2^1 + \frac{1}{3}I_1^0\right)U + \left(\frac{1}{2}I_2^1 - I_3^2\right) = 0. \tag{2.29}$$

Substituting (2.28) into (2.29), we arrive at an equation of instantaneous swimming speed $U(t)$ in terms of integrals I_n^m as

$$U(t) = \frac{I_3^0\left(I_3^2 - \frac{1}{2}I_2^1\right) - I_3^1\left(I_3^1 - \frac{1}{2}I_2^0\right)}{I_3^0\left(I_3^2 - I_2^1 + \frac{1}{3}I_1^0\right) - \left(I_3^1 - \frac{1}{2}I_2^0\right)^2}. \tag{2.30}$$

2.2.1 Swimming Speed for Different Wavenumbers

Since we have found an expression for instantaneous swimming speed at time t, we could use it to evaluate the swimmer's swimming speed for different values of wavenumber κ, and see when the swimmer gets its optimal swimming speed.

We will assume the amplitude of the propelling wave a is not too big, so the swimmer doesn't get pushed too close to the topography. In order to make things simpler, we first try the case when the wavelength of the swimmer, k, and the wavelength of the topography, K, are commensurate, i.e. the wavenumber $\kappa = 1$. Note that since both the shape of the swimmer, $Y(x,t)$, and the shape of the topography, $h(x)$, are fixed for the infinite stiffness case, we could solve all the I_n^m integrals exactly by using the fundamental techniques of integration.

With $Y = a\cos\xi$ and $h = b\cos x - 1$, the distance d in between is

$$d = a\cos(x+\phi) - b\cos x + 1 = C_1\cos(x+\Phi) + 1, \tag{2.31}$$

where $\phi(t)$ measures the phase of translation of the swimmer with respect to the washboard. To sum these two cosine functions, we define $\tan\Phi = \dfrac{\sin\phi}{\cos\phi - \frac{b}{a}}$ and $C_1 = a\sqrt{(\cos\phi - \frac{b}{a})^2 + \sin^2\phi} < 1$. We can evaluate all six integrals, I_n^m, one by one and get

$$I_1^0 = \frac{1}{\sqrt{1 - {C_1}^2}}, \tag{2.32}$$

$$I_3^0 = \frac{1}{2}\cdot\frac{(2 + {C_1}^2)}{(1 - {C_1}^2)^{\frac{5}{2}}}, \tag{2.33}$$

$$I_2^0 = \frac{1}{(1 - {C_1}^2)^{\frac{3}{2}}}, \tag{2.34}$$

$$I_3^1 = \frac{1}{2\pi}\left(\frac{2\pi}{(1 - {C_1}^2)^{\frac{3}{2}}} + b\cos\Phi\left(-\frac{3C_1\pi}{(1 - {C_1}^2)^{\frac{5}{2}}}\right) - \frac{\pi(2 + {C_1}^2)}{(1 - {C_1}^2)^{\frac{5}{2}}}\right), \tag{2.35}$$

$$I_2^1 = -\frac{C_1(C_1 + b\cos\Phi)}{(1 - {C_1}^2)^{\frac{3}{2}}}, \tag{2.36}$$

and

$$I_3^2 = \frac{1}{2\pi}\left[-\frac{2\pi({C_1}^2 + 2C_1 b\cos\Phi + 1)}{(1-{C_1}^2)^{\frac{3}{2}}} + b^2\cos^2\Phi\pi\left(\frac{1+2{C_1}^2}{(1-{C_1}^2)^{\frac{5}{2}}}\right) + b^2\sin^2\frac{\pi}{(1-{C_1}^2)^{\frac{3}{2}}} - 2\left(-\frac{3C_1\pi b\cos\Phi}{(1-{C_1}^2)^{\frac{5}{2}}}\right) + \frac{\pi(2+{C_1}^2)}{(1-{C_1}^2)^{\frac{5}{2}}}\right], \qquad (2.37)$$

where $\sin\Phi$ and $\cos\Phi$ are defined as

$$\sin\Phi = \frac{\sin\phi}{\sqrt{\sin^2\phi + (\cos\phi - \frac{b}{a})^2}} \quad \text{and} \quad \cos\Phi = \frac{\cos\phi - \frac{b}{a}}{\sqrt{\sin^2\phi + (\cos\phi - \frac{b}{a})^2}}.$$

Note the details of calculating the integrals of I_n^m are covered in Appendix A.

Now we substitute all the integral values (2.32)-(2.37) into (2.30) and get an equation of swimming speed U in terms of $\phi(t)$. By taking $a = 0.5$ and $b = 0.4$, we get a plot of instantaneous swimming speed U versus phase translation, $\phi(t)$, for $\kappa = 1$ shown in figure 2.1.

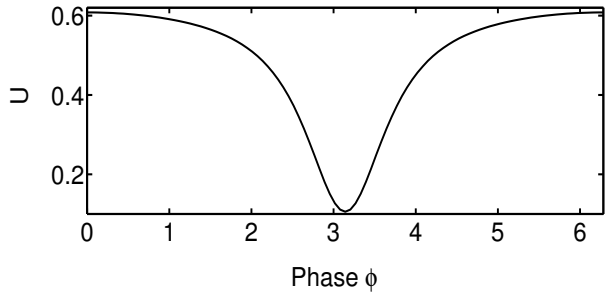

Figure 2.1: A plot of exact instantaneous swimming speed, U, against the phase translation with respect to the washboard, $\phi(t)$, for $a = 0.5$, $b = 0.4$ and $\kappa = 1$.

We then check how the swimming behavior changes as wavenumber changes. Again, we could calculate the exact solution of the swimming speed by evaluating each integral I_m^n as what we did for $\kappa = 1$; however, to save some time, we will use trapezoidal numerical integration on MAT-

LAB instead. The instantaneous swimming speeds for $a = 0.5$ and $b = 0.4$ with different values of wavenumber are represented in figure 2.2. It can be seen that instantaneous swimming speeds behave quite differently for various values of wavenumber.

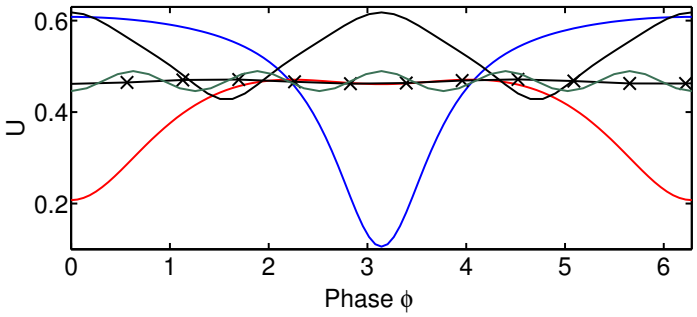

Figure 2.2: Plot of instantaneous swimming speed, U, against the phase translation with respect to the washboard, $\phi(t)$, for $a = 0.5$, $b = 0.4$ and $\kappa = 1$ (blue), 2 (red), 1/2 (black), 4/5 (black with crosses) and 4/9 (green).

There are some interesting limiting cases of instantaneous swimming speed, we will take a look:
Case I (amplitude of the wavy wall approaches to zero, i.e. $b \to 0$):
In this case, $d \to Y$ and (2.28) is reduced to be

$$QI_3^0 + I_2^0 - \frac{U}{2}I_2^0 = 0 \Rightarrow Q = \frac{I_2^0\left(\frac{U}{2} - 1\right)}{I_3^0}. \tag{2.38}$$

Meanwhile, (2.29) is reduced to be

$$\begin{aligned} &\left(\frac{1}{2}I_2^0 - I_2^0\right)Q + \left(I_1^0 - I_1^0 + \frac{1}{3}I_1^0\right)U + \left(\frac{1}{2}I_1^0 - I_1^0\right) = 0 \\ &\Rightarrow -\frac{1}{2}I_2^0 Q + \frac{1}{3}I_1^0 U - \frac{1}{2}I_1^0 = 0. \end{aligned} \tag{2.39}$$

Combing (2.38) and (2.39) and solving for the swimming speed, U, gives

$$U \to \frac{6I_1^0 I_3^0 - 6(I_2^0)^2}{4I_1^0 I_3^0 - 3(I_2^0)^2}. \tag{2.40}$$

Recall that

$$I_1^0 = \frac{1}{\sqrt{1-a^2}}, \quad I_2^0 = \frac{1}{(1-a^2)^{3/2}}, \quad I_3^0 = \frac{2+a^2}{2(1-a^2)^{5/2}}.$$

Plugging in above equations into (2.40), it arrives that

$$U \to \frac{6I_1^0 I_3^0 - 6(I_2^0)^2}{4I_1^0 I_3^0 - 3(I_2^0)^2} = \frac{3a^2}{(1-a^2)^3} \Big/ \frac{1+2a^2}{(1-a^2)^3} \equiv \frac{3a^2}{1+2a^2}. \tag{2.41}$$

It matches with the result of a flat lower surface found by Chan *et al.* [10].
Case II (amplitude of the restoring force approaches to zero, i.e. $a \to 0$):
From our swimming speed equation (2.30), we can see that, as $a \to 0$, $U \to 0$. Physically $a \to 0$ means that the force strength driving the locomotion approaches to zero. As the force strength approaches to zero, it is clear that the swimming speed U will approach to zero.
Case III (sum of the amplitude of the washboard and the amplitude of restoring force approaches to the mean distance between the swimmer and the washboard, i.e. $a + b \to 1$):
As $a + b \to 1$, the swimmer will touch the washboard at some moments during the swimming. It will limit the swimmer's swimming speed. This situation is unphysical in the sense that a divergent force would be required to overcome the resulting lubrication pressures.

2.2.2 Swimming with High Amplitude Force

Note that if $a + b > 1$, the swimmer will finally reach a locked swimming state. It means that the swimmer must stay with a steady swimming speed $U = 1$; otherwise, the swimmer will collide with the washboard. In this situation, (2.30) will not be valid when the swimmer and the washboard collide; however, for other values of phases, the equation (2.30) will still be valid.

Under high amplitude assumption, a plot of instantaneous swimming speed, U, over the acceptable values of phase ϕ for various value of a are shown in figure 2.3 ($b = 0.4$ and $\kappa = 1$ are taken in this example).

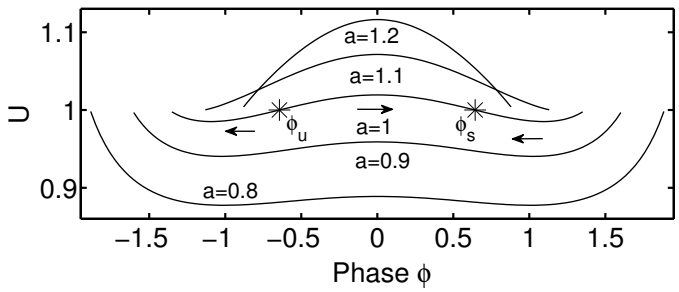

Figure 2.3: Plot of instantaneous swimming speed, U, against the phase translation with respect to the washboard, $\phi(t)$, for $b = 0.4$, $\kappa = 1$ with various values of a indicated. The arrows indicate the moving direction of the swimmer and the two stars on the line $a = 1$ indicate the stable and unstable equilibria.

We can see from figure 2.3 that when a is slightly above the value of $1-b$ (like $a = 0.8$ and $a = 0.9$ in the plot), the swimming speed $U(\phi)$ remains below one over the acceptable range of ϕ, which is below the wavespeed. It indicates that the swimmer always travels in the negative x-direction whenever the swimmer is released in the acceptable range of phase. In the wave frame the swimmer travels in the opposite direction of the washboard. In this situation, the swimmer eventually touches with the washboard after travelling leftwards. Conversely, if a is fairly high (like $a = 1.1$ and $a = 1.2$ in plot), the swimming speed $U(\phi)$ remains above one throughout the admissible range of ϕ. So, the swimmer will always move to the right before touching with the washboard.

Notice that there is a range of forcing amplitude between 0.9 and 1.1 shown in figure 2.3 where instantaneous swimming speed reaches one at two different phases. It suggests that there is a swimming direction change over the acceptable phases. When $U(\phi) < 1$, the swimmer travels to the left for the corresponding phases of ϕ; while it travels to the right whenever $U(\phi) > 1$. In figure 2.3, the two black stars on the curve $a = 1$ indicate the two phases which gives $U(\phi) = 1$. Since when $U > 1$, the swimmer moves to the right and to the left when $U < 1$, the left-hand equilibrium is unstable

(labeled as ϕ_u in the figure) and the star on the right hand side is stable (labeled as ϕ_s in the figure). When these two equilibria points exist, the fate of the swimmer will depend on the condition of initial phase. If the initial phase $\phi_0 > \phi_u$, the swimmer will be converging to the stable fixed point ϕ_s. Or, the swimmer will hit the washboard after moving to the left when $\phi_0 < \phi_u$.

As shown in figure 2.4, the appearance of two equilibria indicates that there is a saddle-node bifurcation in phase ϕ within a certain range of force amplitude a. However, it could be seen that the range where two equilibria exists is very narrow. So, when $a+b>1$, it is most likely that the swimmer will hit the washboard very soon, and result in a steady locomoting state with $U = 1$ and contact.

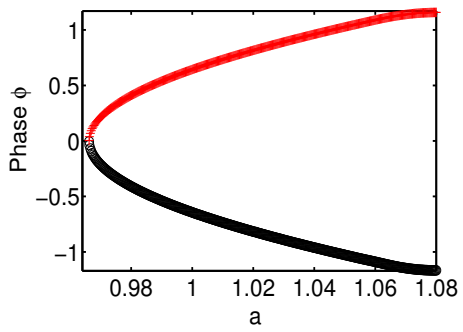

Figure 2.4: Bifurcation diagram of two equilibria phases against the various value of a. The stable solutions are indicated in red crosses, while the unusable solution in black circles.

2.2.3 Average Speed of the Swimmer

When we look at the motion of an object, it is not only important to look at instantaneous swimming speed, but also its overall swimming behavior. For our swimming problem, we already had an expression of swimming speed $U(\phi)$ as shown in equation (2.30), and now we can use it to calculate the average swimming speed $\bar{U}$ over the phase translation ϕ easily. However, it makes more physical sense to look at the average speed over time instead

of over the phase translation. Now we would like to do a simple change of variable and get a new expression of average speed over time.

We have defined the phase translation over the washboard, ϕ, as

$$\phi = t - \int_0^t U(t)\ dt \Rightarrow \frac{d\phi}{1-U} = dt,$$

and we know $\int_0^{2\pi}\ d\phi = 2\pi$ and $\int_0^T\ dt = T$.
Changing variable, it gives an expression of time period in terms of ϕ as

$$T = \int_0^{2\pi} \frac{d\phi}{1-U}.$$

Thus, we can convert average speed over ϕ to be over time t by

$$\bar{U} \equiv \frac{\int U\ dt}{\text{period T}} = \int_0^{2\pi} \frac{U(\phi)\ d\phi}{1-U(\phi)} \Big/ \int_0^{2\pi} \frac{d\phi}{1-U(\phi)}. \tag{2.42}$$

So far, we only focused on the case when the wavenumber $\kappa = 1$. Here, we extend our work to look at more general settings of the wavenumber. To do that, we assume the wavenumber to be a rational number, $\kappa = K/k$. We then compute the integrates in equation (2.42) over the fundamental period, $L = 2\pi k$, of both the forcing and the topography to get the average speed over time for various values of wavenumber. A plot of average Speeds, $\bar{U}$, over various number of wavenumber, κ, is illustrated in figure 2.5 with the same values of a and b as before. We can see that there is a complicated and discontinuous relationship between average speed, $\bar{U}$, and the wavenumber, κ. It doesn't show a clear pattern that how the wavenumber will affect the swimmer's swimming behavior. When $\kappa < 1$, with some choice of wavenumber, there is an increasing of average speed with higher wavenumber. While $\kappa > 1$, for some values of wavenumber, there is a decreasing of average speed with higher wavenumber. We can see that when $\kappa = 1/2$, it gives a fairly high speed. However, $\kappa = 3$, the swimming speed is comparably low. Note that most of the rational wavenumbers lead to similar average swimming speed of about 0.47.

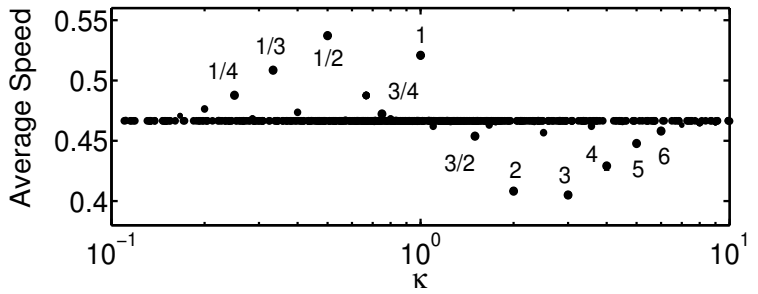

Figure 2.5: A plot of average speed, $\bar{U}$, against various values of wavenumber, κ, with $a = 0.5$ and $b = 0.4$. Some values of the wavenumber are labelled in the figure.

As shown in figure 2.6 and 2.7, there is some dependence of the topographic amplitude (b-dependent) on the relationship between average speed and various values of wavenumber. For $\kappa < 1$, average speed is higher with bigger b value compared to the smaller number of b. In opposite, for $\kappa > 1$, average speed reaches a bigger number for smaller values of b. For $\kappa = 1/n$, where the integer $n \gg 1$, geometrically, we could expect that the topography appears much like a flat underlying plane for a big fraction of the time. With $a = 0.5$, we can see from figure 2.7 that, as n gets bigger, there is a more rapid change of average swimming speed when $b \to \frac{1}{2}$. Actually, for $\kappa = 1/n$, where n is big, we should expect that the average swimming speed, $\bar{U}$, increases to unity as $b \to \frac{1}{2}$, which means that the swimmer reaches its locked state.

2.2.4 General Shape of the Topography

So far, we have assumed that the topography is represented by a simple cosine curve. However, in the real world, the swimming environment for micoorganisms is more complicated than this [34]. Here, we will extend the previous work to a more general topography. Now we redefine the topogra-

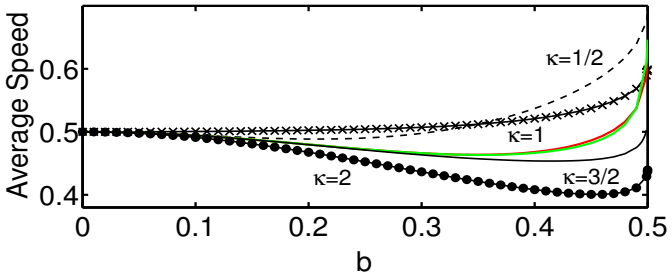

Figure 2.6: A plot of average speed, $\bar{U}$, against various values of topographic amplitude, b, with $a = 0.5$ and different wavenumbers indicated. Note $\kappa = 4/9$ is in red and $\kappa = 4/5$ is in green.

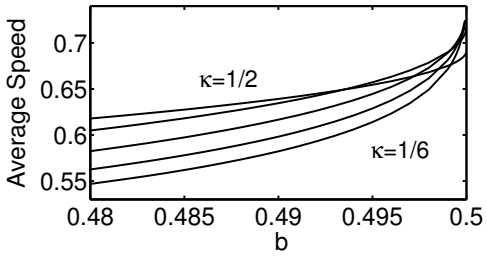

Figure 2.7: A zoomed-in plot of average speed $\bar{U}$ for $\kappa = 1/n$, for $n = 2, 3, \ldots, 6$ (shown from top to bottom) as $b \to \frac{1}{2}$.

phy, $h(x)$, as

$$h(x) = b(1+\alpha) \cdot \frac{\cos \kappa x}{1 + \alpha \cos \kappa x} - 1, \tag{2.43}$$

where b measures the amplitude of the topography, κ is the wavenumber, and α is a parameter that controls the shape of the topography. Note that when $\alpha = 0$, the topography goes back to our original simple cosine shape. With this general topography, our old equation of instantaneous swimming speed $U(t)$ in terms of integrals I_n^m becomes,

$$U(t) = \frac{I_3^0 \left(I_3^2 - \frac{1}{2} I_2^1\right) - I_3^1 \left(I_3^1 - \frac{1}{2} I_2^0\right)}{I_3^0 \left(I_3^2 - I_2^1 + \frac{1}{3} I_1^0\right) - \left(I_3^1 - \frac{1}{2} I_2^0\right)^2}, \tag{2.44}$$

where

$$I_n^m \equiv \left\langle \frac{Y^m}{(Y-h)^n} \right\rangle,$$

is still valid. We also have the equation of average speed

$$\bar{U} \equiv \frac{\int U\ dt}{\text{period T}} = \int_0^{2\pi} \frac{U(\phi)\ d\phi}{1-U(\phi)} \Bigg/ \int_0^{2\pi} \frac{d\phi}{1-U(\phi)} \tag{2.45}$$

as before.

In the following, we will take a look how various values of α changes the swimmer's swimming behaviour. Here, $\alpha = 0.5$ and $\alpha = 2$ are taken as an example. When $\alpha = 0.5$, the geometry of our problem looks like

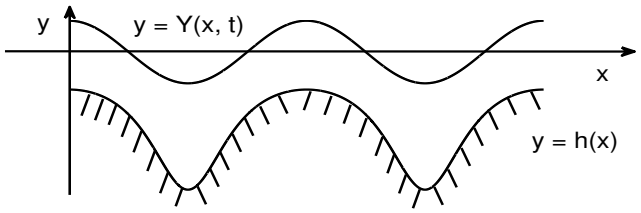

Figure 2.8: Geometry of the problem for $\alpha = 0.5$.

When $\alpha = 2$, the geometry of our problem looks like

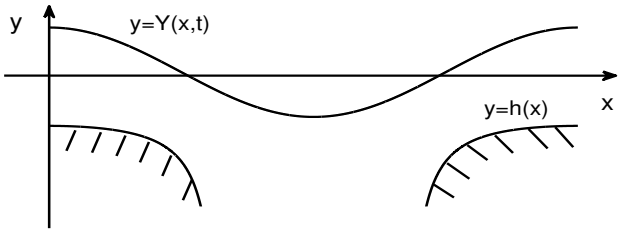

Figure 2.9: Geometry of the problem for $\alpha = 2$.

Note: Here for $\alpha = 2$, the topography is not a continuous wavy shape any more. There is a gap between each periodic section of the topography.

Now, we can use MATLAB to calculate the instantaneous swimming speed of the swimmer, $U(t)$, for various values of α as we did for the simple cosine wave topography. A plot of the instantaneous swimming speed of

the swimmer with forcing amplitude $a = 0.5$, topographic amplitude $b = 0.4$, and wavenumber $\kappa = 1$ is shown in figure 2.10. We can see that the swimmer behaves differently when swimming against the topography with different shapes. It is clear to see that, when α increases from 0 to 0.5, the instantaneous swimming speed at zero phase decreases. When α increases to two, the instantaneous swimming speed at zero phase is even lower. The instantaneous swimming speed is zero for the region when the topography is discontinuous.

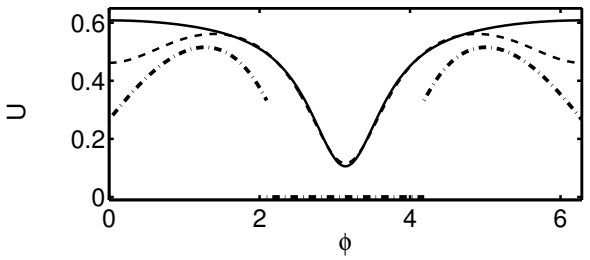

Figure 2.10: A plot for instantaneous swimming speed, $U(t)$, against phase translation with respect to the solid wall, $\phi(t)$, for $a = 0.5$, $b = 0.4$ and $\alpha = 0$ (solid), $\alpha = 0.5$ (dashed) and $\alpha = 2$ (dash-dotted).

The average swimming speed against different values of topographic amplitude for various values of α is shown in figure 2.11. When $\alpha = 0$, the average swimming speed increases as the amplitude of the topography increases. When $\alpha = 0.5$, at first, the average swimming speed increases as the amplitude of the topography decreases. However, as the gap of the swimmer and the topography gets very narrow, the average swimming speed gets higher. It is interesting to see that as the swimmer and the topography get very close, for these two values of α, the average swimming speed converges to the same value. For $\alpha = 2$, the average swimming speed is always increasing with the increasing values of topographic amplitude. However, the averaged swimming speed for this case is always lower than the cases $\alpha = 0$ and $\alpha = 0.5$.

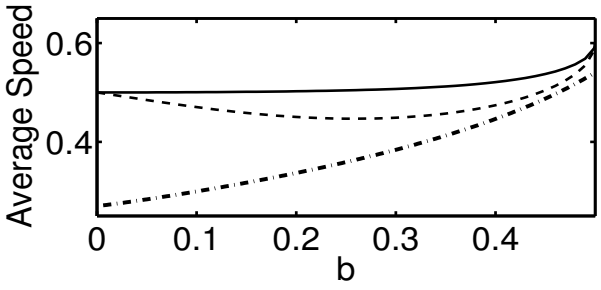

Figure 2.11: A plot for average swimming speed, $\bar{U}$, against various values of the amplitude for the topology, b, for $a = 0.5$, and $\alpha = 0$ (solid), $\alpha = 0.5$ (dashed) and $\alpha = 2$ (dash-dotted).

Chapter 3

Elastic Swimmer with Lubrication Theory Analysis

In this chapter, lubrication theory analysis is again applied. So, the assumption that the mean distance between the swimmer and the washboard, $\bar{d}$, compared with the wavelength of the swimmer, k, is very small is again needed. As in the previous chapter, there is a prescribed normal forcing distributed along the body of the swimmer. However, different from before, we assume the swimmer responds to the applied force as an elastic beam with a finite stiffness. Some work related to our elastic swimmer model has been done previously. In [24], A. E. Hosoi and L. Mahadevan looked at the dynamics of an elastic sheet over a thin layer of fluid under lubrication approximation. In [12], G. J. Elfring and E. Lauga modelled the swimming of spermatozoon using a flexible thin sheet.

In this chapter, we will look at cases where there is a small amplitude or a high amplitude restoring force applied. We will also look at various settings of wavenumbers and various values of stiffness to see how the swimming behaviour changes as things varies. We further compare the results in Chapter Two with the results about this finite stiffness swimmer.

3.1 Mathematical Formulation

In the previous chapter, we looked at the case when the shape of the swimmer is fixed. Here we move on to look at the case where there is an elastic swimmer with a finite stiffness.

Since we still working on the same main problem mentioned in Chapter One with the lubrication approximation applied, everything mentioned in

section 2.1 will continue to be valid. Here, let's recall what we have from section 2.1.

The geometry of the problem in the fixed reference frame will still be the same. Under the lubrication approximation, after non-dimensionalizing, we have the conservation of momentum and the mass equations reduced to be

$$p_x = u_{yy}, \tag{3.1}$$

$$p_y = 0, \tag{3.2}$$

$$u_x + v_y = 0 \tag{3.3}$$

The boundary conditions are

$$u(x, Y) = U(t), \qquad (x, Y) = Y_t + UY_x, \tag{3.4}$$

$$u(x, h) = 0, \qquad v(x, h) = 0. \tag{3.5}$$

Again, if we integrate the conservation of momentum equations with the boundary conditions applied, we get

$$u(x, y) = \frac{1}{2}p_x(y - Y)(y - h) + \frac{U}{Y - h}(y - h). \tag{3.6}$$

Plugging in (3.6) into (3.3) with boundary conditions applied, we get

$$Y_t = \frac{d}{dx}\left(\frac{p_x}{12}(Y - h)^3 - \frac{U}{2}(Y - h)\right). \tag{3.7}$$

The topography is still defined as a cosine wave, like

$$h(x) = b\cos(\kappa x) - 1. \tag{3.8}$$

Moreover, we have the normal force balance condition on the upper surface of the swimmer as

$$p = DY_{xxxx} - f, \tag{3.9}$$

where D is a parameter measuring the stiffness of the swimmer, p is the

pressure, Y is the shape of the swimmer, and f is the applied restoring force, which drives the locomotion of the swimmer. We define the restoring force, f, as

$$f(x,t) = A\cos\left(x - \int_0^t U(\hat{t})\ d\hat{t} + t\right), \tag{3.10}$$

where A denotes the force strength. We assume the restoring force f produces a propagating wave along the swimmer to the negative x direction. Note that here we assume D has an finite value. Plugging in (3.9) into (3.7), we get

$$Y_t = \frac{d}{dx}\left(\frac{(DY_{xxxx} - f)_x}{12}(Y-h)^3 - \frac{U}{2}(Y-h)\right). \tag{3.11}$$

Since the periodicity in pressure condition and the equation of the motion of the swimmer are still valid, we will still have

$$M\dot{U} = -\langle p(x,t)Y_x + u_y(x,Y,t)\rangle. \tag{3.12}$$

Plugging in (3.6) and (3.9) into (3.12), we get a second equation

$$M\dot{U} = -\left\langle \frac{U}{Y-h} - \frac{(DY_{xxxx} - f)_x}{2}(Y-h) + (DY_{xxxx} - f)Y_x \right\rangle. \tag{3.13}$$

Putting (3.11) and (3.13) together, we get a new system of partial differential equations describing the swimmer's shape, Y, and swimming speed, U,

$$\begin{aligned} Y_t &= \frac{d}{dx}\left(\frac{(DY_{xxxx} - f)_x}{12}(Y-h)^3 - \frac{U}{2}(Y-h)\right), \\ M\dot{U} &= -\left\langle \frac{U}{Y-h} - \frac{(DY_{xxxx} - f)_x}{2}(Y-h) + (DY_{xxxx} - f)Y_x \right\rangle. \end{aligned}$$

Because we consider the inertialess limit with $M = 0$, the left hand side of (3.13) will be zero. Furthermore, we assume initially the swimmer is a flat sheet sitting along the x axis with no velocity, i.e. $Y(x,0) = 0$ and $U(0) = 0$.

3.2 Swimming with Finite Stiffness

In this section, we will solve the above system of partial differential equations (equation (3.11) and (3.13)) as an initial value problem in MATLAB. Recall, the initial condition will be $Y(x,0) = 0$ and $U(0) = 0$. The derivatives involved in the equations are computed using the fast Fourier transform algorithm. This system is firstly discretized on the uniform spatial grid and the resulting coupled ordinary differential equations in time would be solved using a standard stiff integrator (MATLAB's ode15s).

We use $D = 1$, $\kappa = 1$ and $b = 0.4$ as an example for the initial value problem. The solution curves for various values of swimming forcing amplitude are shown in figure 3.1. It can be seen that after a very short transient, the solutions converge to a well-defined periodic state. From this figure, we can see that the higher value of the forcing amplitude is the higher the swimming speed and the longer the swimming period are.

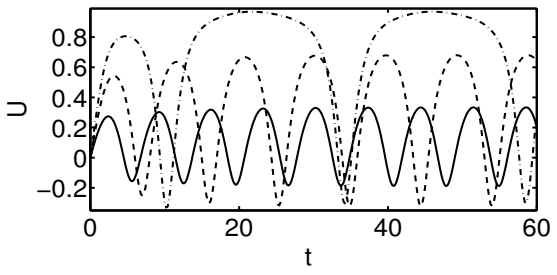

Figure 3.1: A plot of instantaneous swimming speed, $U(t)$, for various values of A with $D = 1$, $\kappa = 1$ and $b = 0.4$. The solid curve is for $A = 2$, dashed curve for $A = 3$ and dashed and dotted curve for $A = 3.8$.

Series snapshots of periodic states with various of A are shown in figure 3.2 panels (a)-(c). We can see that, beginning with a flat sheet, the locomotion makes the swimmer deform into a richer spatio-temporal pattern at the final periodic state. Moreover, as we expected, the bigger the amplitude of the restoring force is, the bigger the amplitude of the locomotive wave is.

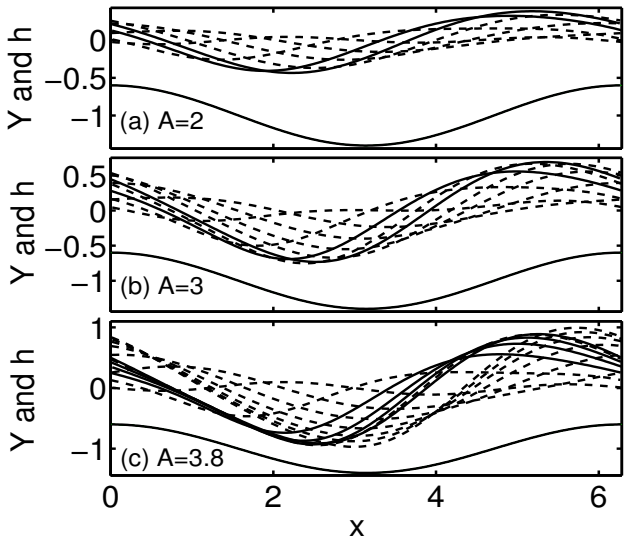

Figure 3.2: A plot displays successive snapshots of the final periodic state for various values of A with $D = 1$, $\kappa = 1$ and $b = 0.4$. Panel (a) is for $A = 2$, (b) for $A = 3$ and (c) for $A = 3.8$.

Now we would like to look for the answer of a key question: whether the washboard will help the swimmer's to swim for this sample case? Recall, as Balmforth *et al.* have found out in a previous paper, in the limit of low amplitude, the swimming speed could be solved analytically by a regular perturbation expansion [3], which gives

$$U \approx \frac{3A^2(1 - e^{-t/M})}{144 + D^2}. \tag{3.14}$$

A plot of mean speed against various values of A is shown in figure 3.3. We can see that, for small values of forcing amplitude, the mean swimming speed increases quadratically as A increases. Moreover, for small values of forcing amplitude, the mean speed solution with topography matches with the solution without topography. It indicates the fact that, for small amplitude locomotive wave over a washboard, the swimming speed gets averaged out to the leading order, so the mean swimming speed shows no difference with the case without topography in figure 3.3. For bigger forcing

amplitude, mean swimming speed with topography increases much more rapidly than the case without topography. For our special choice of stiffness, wavenumber and topography amplitude, it can be seen that the mean speed reaches the wave speed, i.e. $U = 1$, when A is beyond 4, which corresponds to the locked swimming state. In this locked state, the swimmer will be very close to the wavy wall and the lower surface of the swimmer will move like a caterpillar tread over the washboard.

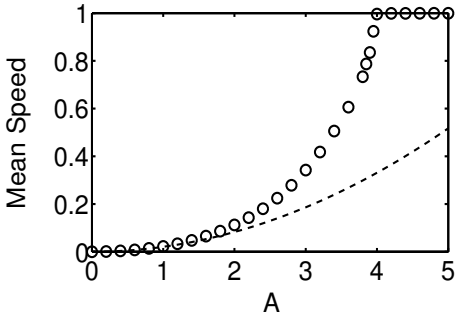

Figure 3.3: Mean speed for the initial value problem against A with $D = 1$, $\kappa = 1$ and $b = 0.4$. The circles indicate the numerical solutions with topography, and the dashed curve indicates the analytical solutions without topography.

A plot of mean speed against topographic amplitude for our special choice of $D = 1$ and $\kappa = 1$ is shown in figure 3.4. Much like the infinite stiffness and $\kappa = 1$ result shown in figure 2.6, mean speed increases with the topological amplitude for all these three values of A. When $A = 2$, as the topographic amplitude b increases, mean swimming speed increases but only by a very small amount. While, for $A = 3$, mean swimming speed increases more rapidly than $A = 2$. It can be seen from the figure that when $b = 0.6$, the swimmer has reached the locked state. When $A = 3.8$, as the topographic amplitude increases, the swimmer also reaches its locked state, but sooner compared to the case $A = 2$. One can say there is some certain forcing amplitude dependence for the critical value of b when the swimmer first runs into the locked state. From this figure, we can conclude for this special choice of D and κ, the swimmer propels itself more effectively over

a washboard compared to the case when there is no topography presented.

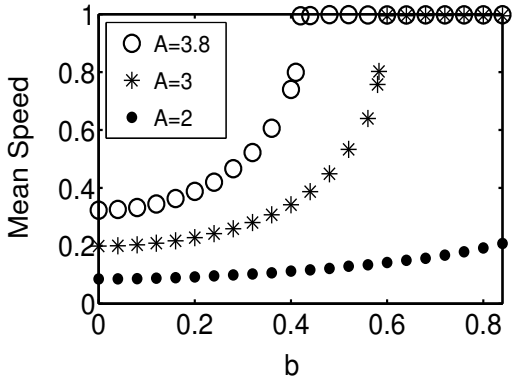

Figure 3.4: Mean speed for the initial value problem against topographic amplitude b with $D = 1$, $\kappa = 1$, and three different values of A are indicated. ($A = 2$ circles, $A = 3$ stars and $A = 3.8$ dots).

3.2.1 Steady Swimming

It has been seen in section 2.2.2 that when the forcing amplitude gets beyond a critical value, the swimmer arrives a locked swimming state. After reaching the locked state, the swimmer keeps a constant swimming speed same as the wave speed, i.e. $U = 1$. So, the locked state is a steady solution in the reference frame of the washboard or the wave. At the locked swimming state, (3.7), (3.9) and (3.12) are still satisfied by the steady swimmer.

Since now the swimmer keep a steady swimming speed of $U = 1$, the time derivative in (3.7) and (3.12) will be zero. That is

$$0 = \frac{d}{dx}\left(\frac{p_x}{12}(Y-h)^3 - \frac{U}{2}(Y-h)\right), \tag{3.15}$$

$$0 = \langle u_y + pY_x \rangle. \tag{3.16}$$

Integrating (3.15) over x, we get a flux equation:

$$Q = \frac{p_x}{12}(Y-h)^3 - \frac{U}{2}(Y-h) \Rightarrow Q = \frac{p_x}{12}(Y-h)^3 - \frac{Y-h}{2}. \tag{3.17}$$

From (3.9), we know that

$$p_x = DY_{xxxxx} + A\sin(x - X), \tag{3.18}$$

where X measures the positional shift of the forcing pattern with respect to the washboard.
Substituting (3.18) into (3.17), we get a differential eigenvalue problem which the steady state swimmer satisfies as

$$Q = \frac{1}{12}(Y-h)^3[DY_{xxxxx} + A\sin(x-X)] - \frac{Y-h}{2}, \tag{3.19}$$

where the eigenvalues we look for are Q and X.

To solve this eigenvalue problem explicitly, we need two additional integral constraints for the eigenvalues. The first one is the speed constraint which comes from (3.16), and the second one is from mass conservation. From (3.16) we have

$$0 = \left\langle \frac{U}{Y-h} + \frac{p_x}{2}(Y-h) \right\rangle - \langle p_x Y\rangle \Rightarrow U = \frac{\left\langle p_x(Y - \frac{Y-h}{2})\right\rangle}{\left\langle \frac{1}{Y-h}\right\rangle} = 1.$$

Thus, the integral speed constraint is

$$\left\langle \left(Y - \frac{Y-h}{2}\right)[DY_{xxxxx} + A\sin(x-X)] \right\rangle = \left\langle \frac{1}{Y-h} \right\rangle. \tag{3.20}$$

The mass conservation gives that

$$\langle Y_t\rangle = \langle Q_x\rangle = \left\langle \frac{d}{dx}\left(\frac{p_x}{12}(Y-h)^3 - \frac{U}{2}(Y-h)\right)\right\rangle.$$

Due to the periodic boundary condition in x direction, it gives $\langle Y_t\rangle = 0$. It means that, over time, $\langle Y\rangle$ is a constant. Thus, the integral mass conservation constraint is

$$\langle Y\rangle = 0. \tag{3.21}$$

The locked state solutions can be computed directly from the eigenvalue problem with these two integral constraints on MATLAB. To get the locked state solutions, we will first solve the initial value problem by doing a spatial discretization with derivatives calculated using the fast Fourier transform. The corresponding time-dependent ordinary differential equation will be solved by the stiff solver (MATLAB's ode15s). Then, we will get the locked solutions by converging the final solution of the initial value problem using Newton's Method.

One sample of the locked state solutions for $D = 1$, $\kappa = 1$ and $b = 0.4$ with various values of A is shown in figure 3.5. Figure 3.5 plots the eigenvalue X along two steady state solutions against forcing amplitude A. It can be seen that the two branches of steady state solutions only exist when the forcing amplitude is beyond some critical value of A_*, which matches with what we have found in the previous subsection. It is clear that the two solutions merge to each other when they approach to the critical value. Finally, the steady state solution will disappear when the forcing amplitude falls below the critical value. Note that, among the two locked state solutions, only the upper branch corresponds to the stable solution as a solution of the initial value problem. One more thing we should notice from figure 3.5 is the behavior of these two locked state solutions indicates a saddle-node bifurcation. The critical threshold value, A_*, denotes the forcing amplitude at which the periodic solutions first locked onto the washboard. To be more specific, if we approaches the critical threshold A_* from below, the periodic oscillatory solution will increase and reach the infinity. This type of saddle-node bifurcation is called saddle-node infinite-period bifurcation, and more information about this type of bifurcation can be found in [38]. This type of bifurcation is seen by Thiele and Knobloch in their study of the depinning process of driven drops on heterogenous substrates [44].

The snapshots demonstrated the final profile of two steady state solutions for two different values of A are shown in figure 3.6. Comparing panel (a) with (b), it can be seen that as the forcing amplitude increases, the swimmer gets pushed closer to the washboard in some sections. Shown in panel (b), the big forcing amplitude leaves a "bubble" of trapped fluid between the

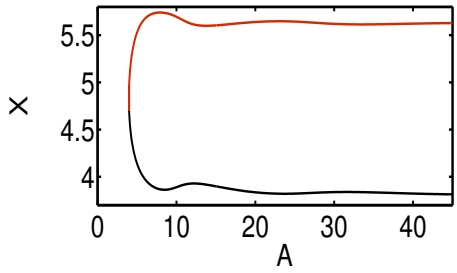

Figure 3.5: The position eigenvalue, X, of two steady state solution branches against A for $D = 1$, $\kappa = 1$ and $b = 0.4$. The upper branch is the stable solution, while the lower one is unstable.

swimmer and the washboard, which has a maximum volume for the stable solution or a minimum volume for the unstable solution. The small cap region is called occluded region and the big "bubble" is called a blister. Analytic expressions of the occlusion and the blister could be calculated using a matched asymptotic expansions method (Takagi and Balmforth in [41]).

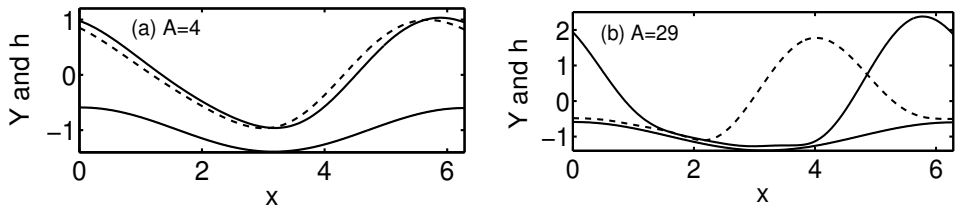

Figure 3.6: Plots of final steady state snapshots of Y and h for $D = 1$, $\kappa = 1$ and $b = 0.4$ with two different values of A. The stable steady state solution is shown by a solid line and the unstable solution is shown by a dashed line.

3.2.2 Larger Stiffness

So far, in the finite stiffness section, we only examined the case when $D = 1$. It will be interesting to take a look at larger stiffness and see how stiffness solutions relate to low stiffness solutions and whether larger stiffness solutions show some similarities to the infinite stiffness results. In this subsection, we

look at the case for the elastic swimmer with larger stiffness. However, for simplicity, we will only consider the wavenumber to be one in the following discussion.

Figure 3.7 displays the instantaneous swimming speeds of the case $D = 100$ with three different values of the forcing amplitude a. Shown in panel (a) and (b), when $a = 0.4$ and $a = 0.8$, the swimmer stays in a periodic swimming state after a very short transition period, which is similar with what we have seen for $D = 1$ (shown in figure 3.1). If the force is sufficiently big, the swimmer gets locked onto the washboard and swims at the unit speed again (displayed in panel (c)). It has been seen earlier that the bigger the forcing, the bigger the swimming speed is.

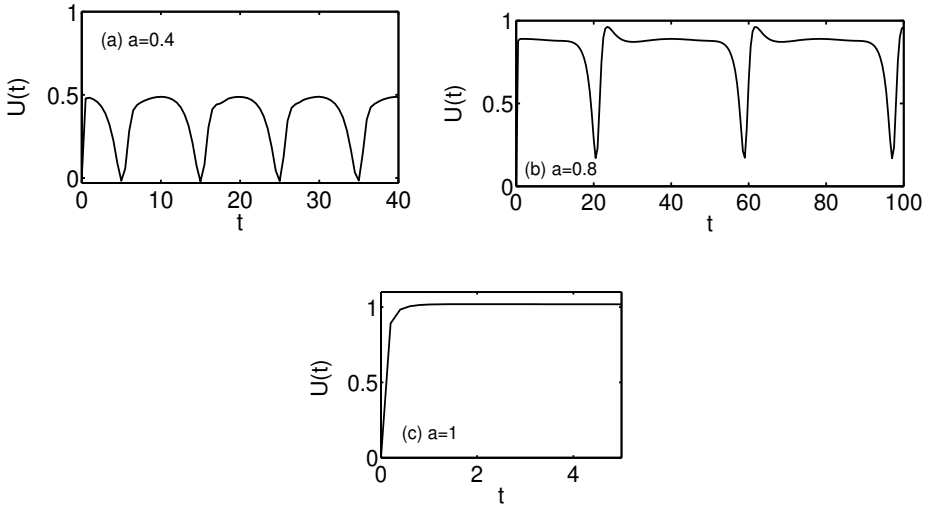

Figure 3.7: Plots of instantaneous swimming speed over time with $D = 100$, $\kappa = 1$ and $b = 0.4$. Panel (a) is the result for $a = 0.4$, (b) for $a = 0.8$ and (c) for $a = 1$.

Figure 3.8 shows the swimmer's profiles over time for two different values of a with $D = 100$, $\kappa = 1$ and $b = 0.4$. Panel (a) displays the case for $a = 0.4$. For this case, the swimmer translates like a simple sine wave. It also shows a noticeable decreasing of swimming speed when the swimmer travels over the crest of the topography, which could be demonstrated in figure 3.7 panel (a).

Recall, we have found in the previous chapter that for the case of infinite stiffness with $\kappa = 1$ and $b = 0.4$, the swimmer collides with the washboard when $a > 0.6$. Presented in panel (b) of figure 3.8, the shape of the swimmer deforms significantly when it approaches the crest of the topography, and it translates like a sine wave elsewhere. Two steady state solutions for $a = 1$ are shown in figure 3.9. Notice that these two steady solutions are similar to the results shown in figure 3.6 for $D = 1$. Moreover, these two steady state solutions look nearly symmetric, which is similar to the case of the finite stiffness swimmer shown in figure 2.3.

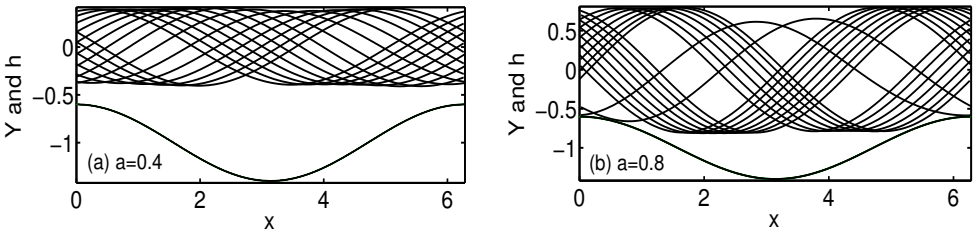

Figure 3.8: Plots show the translation of the swimmer Y over the wavy wall in time for $D = 100$, $\kappa = 1$ and $b = 0.4$ with two different values of a. Panel (a) is the result for $a = 0.4$ and (b) for $a = 0.8$.

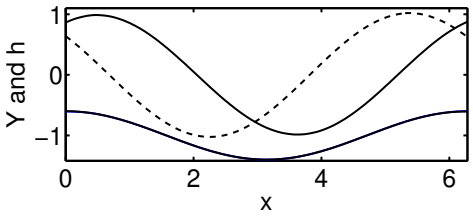

Figure 3.9: A plot of steady state solutions for $a = 1$ when $D = 100$, $\kappa = 1$ and $b = 0.4$. The stable branch is illustrated in solid, and the unstable one is dashed.

Figure 3.10 demonstrates the differences in mean speed for different values of stiffness when the swimmer swims with or without topography. When the swimmer swims over a washboard, we can see that the mean swimming speed is higher for $D = 100$ compared to $D = 10$. For low forcing ampli-

tude, the swimming speed with topography (shown using markers) matches with the speed without the topography (shown in dashed line) for both stiffness values. For high forcing amplitude, when $D = 10$, we observe a big difference between the swimming speed with topography and without topography. However, for $D = 100$, there is no big difference and it will reach unity swimming speed for swimming with topography and without topography. Note that for both $D = 10$ and $D = 100$, the swimmer reaches the locked state for high forcing amplitude when swimming over the washboard. We also see that, for low forcing amplitude, mean swimming speed for finite stiffness swimmer matches with the speed for $D = 100$. However, for high forcing amplitude, the infinite stiffness swimmer will collide with the topography and be a steady state swimmer. For the finite stiffness swimmer, the swimmer will never touch the topography and the steady swimming state connects with the periodic swimming state through a saddle-node infinite-period bifurcation.

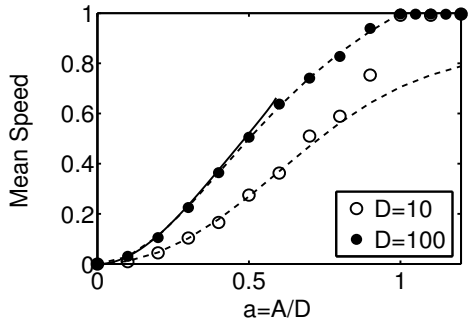

Figure 3.10: Mean swimming speed against various forcing amplitude a for large stiffness swimmer with $\kappa = 1$ and $b = 0.4$. Dots and circles are the solutions with topography for $D = 100$ and $D = 1$ respectively. Dashed line are the solutions without topography (upper one for $D = 100$ and lower one for $D = 10$). The solid line is the solution for infinite stiffness.

To see how large stiffness steady state solutions connect with the steady state solutions for finite stiffness swimmer, a figure of positional shift X against stiffness D is shown in figure 3.11. In order to do a comparison

with steady state solutions for finite stiffness swimmer shown in figure 2.3, we kept $a = A/D = 1$. We can see that the stable steady state solution converges to a positional shift with respect to the washboard of about 0.5 as D increases, and the unstable steady state solution converges to a shift of about -0.5, which matches with what we found for the finite stiffness swimmer (shown in figure 2.3).

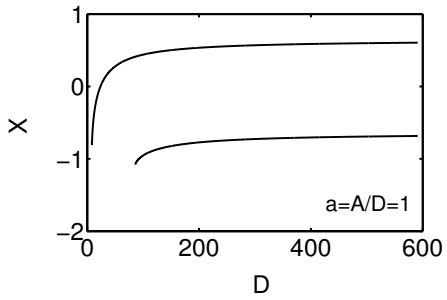

Figure 3.11: A plot of two steady state solutions against D when the forcing amplitude a kept to be 1, $\kappa = 1$ and $b = 0.4$. The upper branch is a stable solution and the lower one is unstable.

3.2.3 Various Values of Wavenumber

For now, we have assumed wavenumber $\kappa = 1$. It will be meaningful to extend our discussion to a more general setting of the wavenumber and check whether the washboard helps increase the swimmer's swimming speed in general.

Figure 3.12 presents the mean swimming speeds for the high stiffness swimmer with a fixed forcing amplitude $a = 0.5$ for various values of wavenumber against b. Here, we specially pick the stiffness $D = 1000$. Comparing with the case of the fixed shape swimmer shown in figure 2.6, we can see a similar dependence of the topographic amplitude (b-dependent) on the relationship between average speed and various values of wavenumber is also shown up here. When $\kappa < 1$, mean speed of the swimmer is increasing with the increasing values of the topographic amplitude. On the other hand, when $\kappa > 1$, there is a higher mean speed of the swimmer for smaller

topographic amplitude.

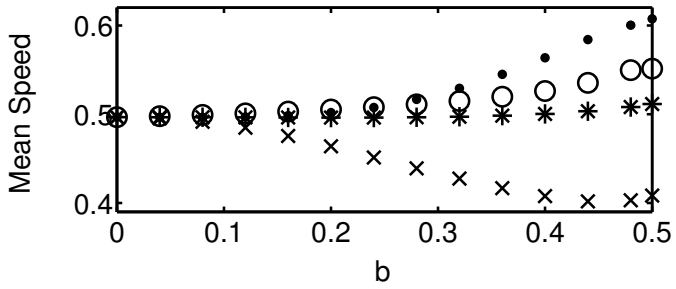

Figure 3.12: A plot show mean speed against b of $a = 0.5$ for four different values of wavenumber ($\kappa = 1/2$ is represented by dots, $\kappa = 1$ by circles, $\kappa = 4/5$ by stars and $\kappa = 2$ by crosses) with $D = 1000$.

In the following, we pick two special choices of wavenumber, i.e. $\kappa = 2$ and $\kappa = 1/2$ to do further analysis. Here, we will do detailed analysis for both these two values of wavenumber and compare their results with the case when wavenumber $\kappa = 1$ and the fixed shape swimmer.

Case I ($\kappa = 2$):

Mean speed and the positional shift versus various values of A for $\kappa = 2$ with $D = 1$ and $b = 0.4$ are displayed in figure 3.13. Recall, in figure 2.6, it has been shown that, with infinite stiffness, the swimming is less effective over the washboard than without washboard when $\kappa = 2$. However, as shown in figure 3.13, the situation with finite stiffness for $\kappa = 2$ is more complicated comparing with the infinite stiffness case or $\kappa = 1$. Again, for low forcing amplitude, the solution is periodic. As an example, the swimmer's profile for $A = 5$ is displayed in panel (a) of figure 3.14. In this regime, the swimmer actually swims faster without the washboard (indicated in figure 3.13 panel (a)). We could say the washboard retards the swimmer for this range of forcing amplitude. As we increase the forcing amplitude, the swimming speed increases abruptly to unity while the swimmer reaches the locked state (an example for $A = 20$ is shown in panel (c) of figure 3.13). An example of two steady state solutions when swimming with washboard for $A = 8$ is shown in figure 3.14 panel (b). In this high forcing amplitude region, mean

speed for swimming without topography decreases because the swimmer is pushed too close to the wall [3]. Notice that the swimmer reaches its locked state sooner for $\kappa = 1$ comparing with $\kappa = 2$.

One interesting thing we should see from figure 3.13 in panel (a) is that the transition between periodic solution and locked state solution is discontinuous for $\kappa = 2$. Comparing the low amplitude periodic solution with the bifurcation diagram shown in figure 3.13 panel (b), it suggests that there is a region (A between 6 and 8) where the periodic and locked states co-exist. The periodic and locked state solutions for this region are shown in the mean speed plot. It is also interesting to see that, for swimming with a topography, if the forcing amplitude goes beyond $A = 22$, we would see the locked state disappeared due to a second saddle-node infinite-period bifurcation. In this region, mean swimming speed decreases and the swimmer goes back to the periodic state (an example for $A = 30$ is shown in panel (d) of figure 3.13).

Case II ($\kappa = 1/2$):

As shown in figure 2.6, the washboard helps with swimming of $\kappa = 1/2$ for the infinite stiffness swimmer. As the topographic amplitude increases, the swimming speed increases. Someone may predict the same thing will happen for the finite stiffness swimmer; however, the situation is more complicated for the finite stiffness swimmer than the infinite stiffness swimmer.

The periodic solutions for $\kappa = 1/2$ and $b = 0.4$ when $D = 1$ are shown in figure 3.15. It is indicated in panel (a) of figure 3.15 that the elastic swimmer is not able to push itself neither more or less effectively over the washboard than the flat wall. At low forcing amplitude, mean speed for $\kappa = 1/2$ is similar with the swimming speed for $\kappa = 1$. As forcing amplitude increases, mean speed for $\kappa = 1$ increases more rapidly than mean speed for $\kappa = 1/2$. An example of the swimmer's periodic swimming profile with $A = 3$ is shown in panel (b) of figure 3.15.

Note that for high forcing amplitude, the subharmonic instability shows up for the periodic swimmer with $\kappa = 1/2$. So, there are two periodic solution branches showing up in panel (a) of figure 3.15. An example of subharmonic instability solutions with $A = 6$ are displayed in figure 3.16.

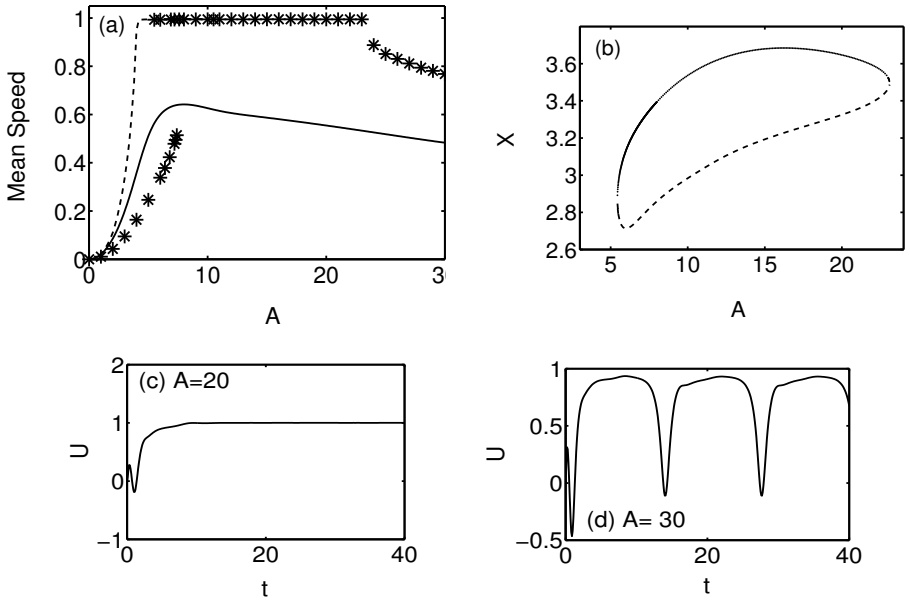

Figure 3.13: Solutions for $\kappa = 2$ and $D = 1$ versus varying A. Panel (a) shows mean speeds for the initial value problem. The stars are the result for $\kappa = 2$ and $b = 0.4$, the solid line shows the result for $\kappa = 2$ without topography, and the dashed line shows the result for $\kappa = 1$ and $b = 0.4$. Panel (b) displays the positional shift, X, versus varying A. The solid branch is the stable steady state solution and the dashed line is the unstable steady state solution.

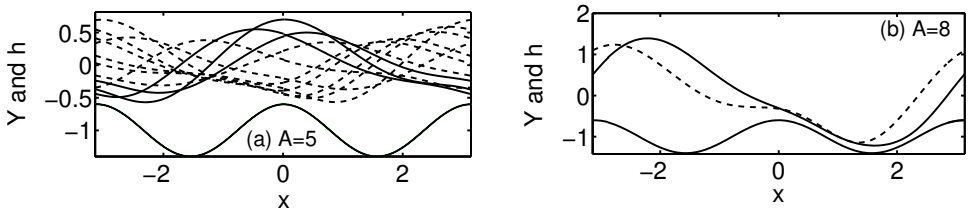

Figure 3.14: Profiles of the swimmer for two special choices of A. Panel (a) demonstrates the periodic solution for $A = 5$ and panel (b) displays the stable steady state solution (solid) and the unstable steady state solution (dashed) for $A = 8$.

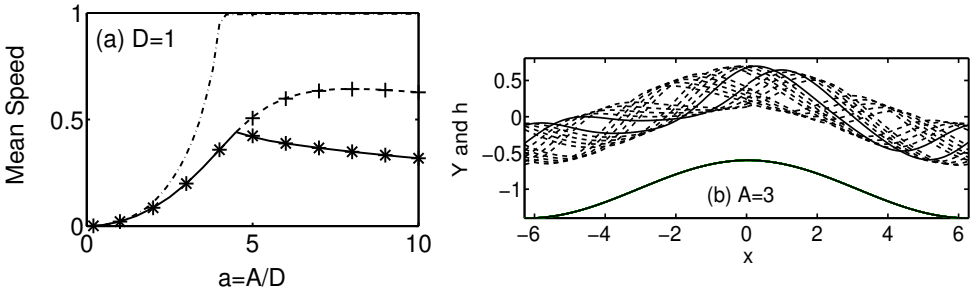

Figure 3.15: Solutions of the initial value problem for $\kappa = 1/2$ when $D = 1$. Panel (a) shows the mean speed for various A. Stars indicate the stable solutions with $b = 0.4$, and plus are unstable solutions with $b = 0.4$. Solid line is the stable solution without washboard and dashed line is the unusable solution without washboard. The dash-dotted line is the solution for $\kappa = 1$. Panel (b) displays the swimmer's profile for the periodic solution when $A = 3$.

From panel (a), we observed a clear change of the swimmer's profile over time. Initially, the swimmer begins with a two-humped wave. The swimmer's profile is shown in panel (b) for this unstable periodic solution. Then, the two humps merge to each other and combined to a single-humped wave at about time $t = 550$. The swimmer's profile is shown in panel (c) for the stable periodic solution. This phenomenon is called a subharmonic instability. Note that this instability happens for both the cases with topography and without topography, and mean speed solutions for both cases are presented in figure 3.15 panel (a).

When the stiffness gets higher, we found that the situation for the high stiffness swimmer is more complicated than the low stiffness swimmer. The mean speed for the swimmer with $D = 10$ is shown in figure 3.17 panel (a). Note that, when the swimmer swims over a washboard, only the stable solutions are displayed in the plot. We see that, for this stiffness, it doesn't seem the washboard helps with the swimming speed. For this stiffness, the swimmer never reaches the locked state. It is shown that a subharmonic instability happens for swimming without washboard within the range $a = 1.1$ and $a = 1.4$ (shown in the inset of panel (a)). If we pull the stiffness even

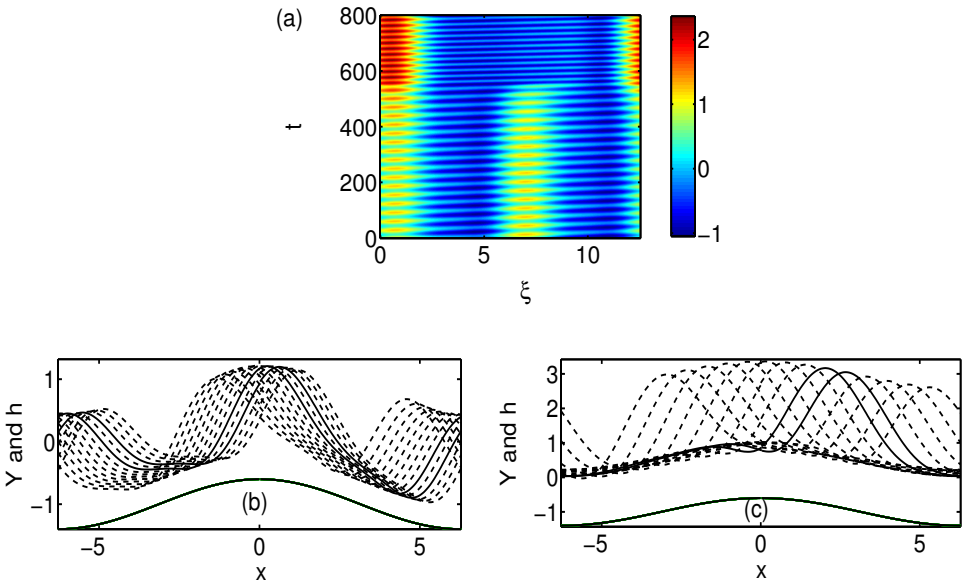

Figure 3.16: Periodic solutions of $\kappa = 1/2$ with $D = 1$, $A = 6$ and $b = 0.4$. Panel (a) shows the evolution of the swimmer's surface, $Y(\xi, t)$, on the (ξ, t) plane. Panel (b) displays the unstable periodic profile for $A = 6$. Panel (c) shows the stable periodic profile for $A = 6$.

higher to be 100, the things get more interesting and complicated as shown in panel (c). For very low forcing amplitude, again mean speed is about the same for swimming with washboard or without washboard. However, unlike what happens to the low stiffness case, for high forcing amplitude, the washboard actually helps the swimmer to swimming more effectively. The swimmer swimming with topography actually reaches the locked state for this stiffness number which is not seen for low stiffness. In this situation, it is also seen that the $\kappa = 1/2$ swimmer with washboard swims faster than the $\kappa = 1$ swimmer for some values of forcing amplitude. Notice that, like before, the subharmonic instability is shown when a is between 0.7 and 1.1 for the swimmer without topography. The inset of (b) gives a bifurcation diagram of the positional shift, X, of the steady state solutions versus forcing amplitude

a. Note the stable solution is shown in solid and the unstable solution is shown in dashed curve. It can be seen that the bifurcation structure is much more complicated for $\kappa = 1/2$ than what happens for $\kappa = 2$ and $\kappa = 1$. We take $A = 105$, i.e. $a = 1.05$, as an example and we can see from the bifurcation diagram that there are four steady state solutions for this value (three unstable solutions and one stable solution). The swimmer's profiles of the steady state solutions at $A = 105$ are displayed in panel (c), where only the solid curve is the stable solution and the rest are unstable solutions.

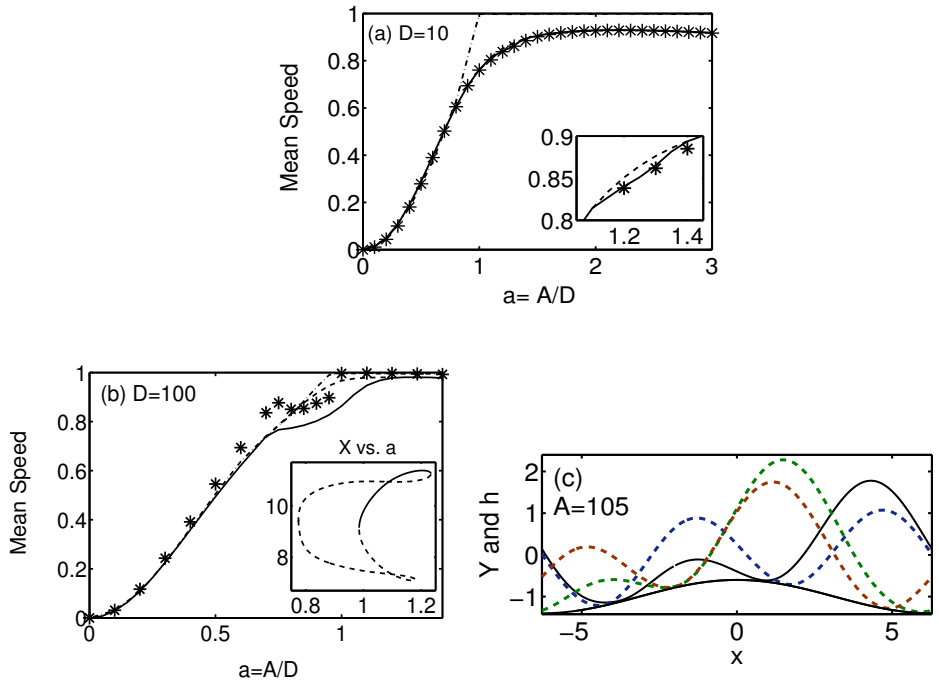

Figure 3.17: The solutions of the initial value problem for $\kappa = 1/2$ with $D = 10$ and $D = 100$. Panel (a) shows mean speed for $D = 10$ against a. Panel (b) shows mean speed for $D = 100$ against a. In both panel (b) and (c), the stars mark the stable solutions with topography. The solid and dashed line show the stable and unstable periodic solutions without topography respectively. The dash-dotted line displays the result for $\kappa = 1$. The inset of (b) shows the positional shift, X, of the four locked state solutions versus the forcing amplitude a for the swimmer swims with topography when $D = 100$. Panel (c) shows the four steady state solution profiles for $A = 105$ and $D = 100$. Only the solid curve is the stable solution and the rest are three unstable solutions.

Chapter 4

Conclusion

In this thesis, we extended a problem analyzed by G. I. Taylor [42] and D. F. Katz [25] to the situation where there is a microorganism swimming very close to a washboard. In this problem, we model the swimmer to be a two-dimensional, infinite periodic waving sheet. For simplicity, we only consider the case where the fluid between the swimmer and the washboard is Newtonian and incompressible. We assume that the swimmer propagates waves along its body and propels itself in the opposite direction. In this chapter, we summarize all the results and described what work could be done in the future.

4.1 Summary of Results

To begin with our problem, we first assumed the swimmer had a known fixed sine wave shape. We first looked for the instantaneous swimming speed of the swimmer with various values of wavenumber. Here the case when the wavenumber $\kappa = 1$ was calculated analytically, while other values of wavenumber was calculated numerically. With amplitude of the resorting force a picked to be 0.5 and amplitude of the topography b picked to be 0.4, we saw the instantaneous swimming speed behaved quite differently for various values of the wavenumber. No clear pattern was shown here. When we looked at the limiting case where the amplitude of the wavy wall approached to zero, i.e. $b \to 0$, we found the swimming speed $U \to \dfrac{3a^2}{1+2a^2}$, which matched with the result of a flat lower surface found by Chan *et al.* [10]. It can easily be seen that as the amplitude of the restoring force approached to zero, i.e. $a \to 0$, the swimming speed U approached to zero. When the sum of the amplitude of the washboard and the amplitude of the

restoring force approached to the mean distance between the swimmer and the washboard, i.e. $a + b \to 1$, the swimmer will touch with the washboard at some moments which limited the swimmer's swimming speed.

Next, we particularly looked at the case when the swimmer swam with a high amplitude force which gave $a + b > 1$. In this situation, the instantaneous speed formula, i.e. equation (2.30), was still valid when there was a open gap between the swimmer and the washboard. Taking $b = 0.4$ and $\kappa = 1$ as an example, we found when a was slightly above the value of $1 - b$, the swimming speed remained below one over the acceptable range of ϕ, which meant the swimmer always travelled to the left. While a was very high, the swimming speed remained above one. So, the swimmer always travelled to the right. It was found that there was a small region of a between 0.9 and 1.1 where the instantaneous swimming speed reached one at two different phases. It suggested that there was a swimming direction change over time. So, in this situation, the swimming behaviour of the swimmer would depend on the condition of the initial phase.

We also looked at the average swimming speed of the swimmer over different values of wavenumber. When $a = 0.5$ and $b = 0.4$ was examined, it didn't shown a clear pattern that how the wavenumber affected the swimmer's swimming behaviour. However, it was interesting to see that when $\kappa = 3$ average swimming speed was comparably low and $\kappa = 1/2$ gave a fairly high swimming speed. It was also found there was some dependence of the topographic amplitude b on the relationship between average speed and the various values of the wavenumber. When $\kappa < 1$, average swimming speed was higher with larger value of b. In opposite, for $\kappa > 1$, average swimming speed was bigger for smaller values of b.

Finally, we checked general shapes of the washboard, which was defined as $h(x) = b(1 + \alpha)\frac{\cos \kappa x}{1+\alpha \cos \kappa x} - 1$. Here the α is the parameter controlling the shape of the washboard. Note when $\alpha = 0$, the washboard went back to be the simple cosine shape washboard. We first looked at the instantaneous swimming speed of the swimmer with forcing amplitude $a = 0.5$, topographic amplitude $b = 0.4$, and wavenumber $\kappa = 1$. We saw the swimmer behaved differently when swimming against the topography with different shapes.

We found that as the values of α increased, the instantaneous swimming speed at zero phase decreased. We then checked the average swimming speed against different values of topographic amplitude for various values of α. We found that, for $\alpha = 0$ and 0.5, as the swimmer and the topography got very close, the average swimming speed converged to the same value. The averaged swimming speed for $\alpha = 2$ was always lower than the cases $\alpha = 0$ and 0.5.

In addition to the case when the swimmer had a fixed known shape, we looked at the case of an elastic swimmer in Chapter Three. We first picked $D = 1$, $\kappa = 1$ and $b = 0.4$ as an example. When the amplitude of the restoring force was small, after a very short transient, the swimmer stayed in a well-defined periodic state. When the amplitude of the restoring force was small, the mean speed of the swimmer with topography matched with the solution without topography. It increased quadratically as A increased. While for bigger forcing amplitude, the mean speed with topography increased much more rapidly than without topography. The mean speed of the swimmer with topography stayed with unity after some critical value of forcing amplitude A_*. We specially looked at this high forcing amplitude swimmer and found there were two branches of steady state solutions existing after reaching this A_*. This phenomenon could be explained by the saddle-node infinite-period bifurcation. We also tried various values of amplitude of the topography and saw the mean speed increased with the topographical amplitude for $A = 2$, 3 and 3.8.

Next, we varied the values of the stiffness. When $D = 100$, same as $D = 1$, the swimmer stayed as periodic when A is small. While reached the steady state with a high forcing amplitude. Looking at the cases for $D = 100$ and $D = 10$, we saw, for small forcing amplitude, mean speed with topography matched with the mean speed without topography for both stiffness. While for high forcing amplitude, it showed a big difference between mean speed with topography and without topography when $D = 10$. However, no big difference was shown for $D = 100$. As stiffness increased, the steady state solutions converged to the steady state solutions of the fixed shape swimmer.

Finally, we examined various values of wavenumber to see how it af-

fected the swimming behaviour. When $\kappa = 2$, with $D = 1$, we saw, having low forcing amplitude, the swimmer swam periodically. In this regime, the swimmer actually swam faster without the washboard. As forcing amplitude increased, the swimmer reached the locked state when swimming with the topography. After doing the bifurcation analysis, it was interesting to see that when A was between 6 and 8, the periodic and locked swimming solutions co-existed. Due to the second saddle-node infinite-period bifurcation happening for this wavenumber, the swimmer went back to the periodic swimming state with a very high forcing amplitude. The situation for $\kappa = 1/2$ was way more complicated compared to $\kappa = 2$. We saw for this value of wavenumber, the swimmer wasn't able to push itself neither more or less effectively over the washboard than the flat wall. At low forcing amplitude, mean speed for $\kappa = 1/2$ was similar with the swimming speed for $\kappa = 1$. While for high forcing amplitude, subharmonic instability showed up. We tried pulling up the stiffness number for this wavenumber, and found when $D = 10$, the washboard didn't help with the swimming at all. When $D = 100$, for high forcing amplitude, unlike the small stiffness case, the washboard actually helped the swimmer to swimming more effectively. It was also found that for this stiffness value the bifurcation structure was very complicated.

4.2 Future Work

Lots more work could be done beyond this thesis. It has been mentioned in the literature that microorganisms frequently experience complex fluids[32, 45]. However, this thesis only examined the situation of Newtonian fluids. From a biological perspective, it will be good if we can extend this work to complex fluids. Moreover, in this thesis, we assumed the swimmer is an infinite length waving sheet. However, in the real world, swimmer always has a finite length. It will be good if we could look at the situation of a finite swimmer as shown in [3]. Another thing mentioned in the paper written by Majmudar *et al.* is that in nature there are many instances where swimming microorganisms must make their way through a fluid embedded with

obstacles [34]. However, in this thesis, we mostly looked at the topography as a cosine curve. A general shape of the topography was only looked at for the case of the fixed shape swimmer. We should also extend our work to look at a general shape of the topography for the elastic swimmer. To be more realistic, we could even extend the work to feature complex fluids setting and a general shape of the washboard.

So far, our analysis has been limited to the case where there is a very thin gap between the swimmer and the topography. It will be interesting to examine other cases. For example, we could attempt biharmonic analysis (done by Katz in [25]) for our problem. We could even further extend our model to the case where the gap between the swimmer and the topography is not small and we do not have a small amplitude swimmer. In the elastic swimmer chapter, we have found that for high values of forcing amplitude, the swimmer got pushed close to the washboard, while the big forcing amplitude also left a bubble of trapped fluid between the swimmer and the washboard. The small cap region is called an occluded region and the big bubble is called a blister. We see the work of asymptotic analysis about this "occluded and blistered" region have been done for the case when swimming near a flat plane in [3]. Here we could follow the same analysis for our problem to get some inside understanding of this behaviour analytically, we could further compare the analytic solution with our numerical solution.

Bibliography

[1] B. Alberts, A. Johnson, J. Lewis, M. Raff, K. Roberts, and P. Walter. *Molecular Biology of the Cell*. Garland Science, New York, 2007.

[2] R. M. Alexander. *Locomotion of animals*. Chapman and Hall, New York, 1982.

[3] N. J. Balmforth, D. Coombs, and S. Pachman. Microelastohydrodynamics of swimming organisms near solid boundaries in complex fluids. *Q. J. Mech. Appl. Maths*, 63:267–294, 2010.

[4] J. R. Blake. Infinite models for ciliary propulsion. *J. Fluid. Mech.*, 49:209 – 222, 1971.

[5] J. R. Blake. Self propulsion due to oscillations on the surface of a cylinder at low reynolds number. *Bull. Austral. Math. Soc.*, 5:255 – 264, 1971.

[6] J. R. Blake. A spherical envelope approach to ciliary propulsion. *J. Fluid. Mech.*, 46:199 – 208, 1971.

[7] J. R. Blake. A model for the micro-structure in ciliated organisms. *J. Fluid. Mech.*, 55:1– 23, 1972.

[8] J. R. Blake. A finite model for ciliated micro-organisms. *J. Biomechanics.*, 6:133 – 140, 1973.

[9] J. R. Blake and M. A. Sleigh. Mechanics of ciliary locomotion. *Biol. Rev.*, 49:85 – 125, 1974.

[10] B. Chan, N. J. Balmforth, and A. E. Hosoi. Building a better snail: Lubrication and adhesive locomotion. *Phys. Fluids*, 17(11):113101.1–113101.10, 2005.

[11] S. Childress. *Mechanics of swimming and flying.* Cambridge Univeristy Press, Cambridge, 1981.

[12] G. J. Elfring and E. Lauga. Synchronization of flexible sheets. *J. Fluid. Mech.*, 674:163 – 173, 2011.

[13] L. J. Fauci. A computational model of the fluid dynamics of undulatory and flagellar swimming. *Amer. Zool.*, 36(6):599 – 607, 1996.

[14] L. J. Fauci and R. Dillon. Biofluidmechanics of reproduction. *Annu. Rev. Fluid. Mech.*, 38:371 – 394, 2006.

[15] L. J. Fauci and A. Macdonald. Sperm motility in the presence of boundaries. *Bull. Math. Biol.*, 57(5):679 – 699, 1995.

[16] J. Gray. Studies in animal locomotion: I. The movement of fish with special reference to the eel. *J. Exp. Biol.*, 10:88 – 104, 1933.

[17] J. Gray. Studies in animal locomotion: II. The relationship between waves of muscular contraction and the propulsive mechanism of the eel. *J. Exp. Biol.*, 10:386 – 390, 1933.

[18] J. Gray. Studies in animal locomotion: III. The propulsive mechanism of the whiting (gadus merlangus). *J. Exp. Biol.*, 10:391– 400, 1933.

[19] J. Gray. Studies in animal locomotion: IV. The neuromuscular mechanism of swimming in the eel. *J. Exp. Biol.*, 13:170– 180, 1936.

[20] J. Gray. Studies in animal locomotion: V. Resistance reflexes in the eel. *J. Exp. Biol.*, 13:181– 191, 1936.

[21] J. Gray. Studies in animal locomotion: VI. The propulsive powers of the dolphin. *J. Exp. Biol.*, 13:192 – 199, 1936.

[22] J. Gray and G. J. Hancock. The propulsion of sea-urchin spermatozoa. *J. Exp. Biol.*, 32:802–814, 1955.

[23] M. M. Hopkins and L. J. Fauci. A computational model of the collective fluid dynamics of motile microorganisms. *J. Fluid. Mech.*, 455:149 – 174, 2002.

[24] A. E. Hosoi and L. Mahadevan. Peeling, healing, and bursting in a lubricated elastic sheet. *Phys. Rev. Lett.*, 93(13):137802.1–137802.4, 2004.

[25] D. F. Katz. On the propulsion of micro-organisms near solid boundaries. *J. Fluid Mech.*, 64(1):33–41, 1974.

[26] D. F. Katz. Characteristics of sperm motility. *Ann. N. Y. Acad. Sci.*, 637:409 – 423, 1991.

[27] D. F. Katz, T. D. Bloom, and R. H. BonDurant. Movement of bull spermatozoa in cervical mucus. *Biol. Reprod.*, 25:931 – 937, 1981.

[28] D. F. Katz, R.N. Mills, and T. R. Pritchett. The movement of human spermatozoa in cervical mucus. *J. Reprod. Fert.*, 53:259– 265, 1978.

[29] D. F. Katz and R. Yanagimachi. Movement characteristics of hamster and guinea pig spermatozoa upon attachment to the zone pellucida. *Biol. Reprod.*, 25:785 – 791, 1981.

[30] S. R. Keller and T. Y. Wu. A porous prolate-spheroidal model for ciliated micro-organisms. *J. Fluid. Mech.*, 80(2):259 – 278, 1977.

[31] E. Lauga. Propulsion in a viscoelastic fluid. *Phys. Fluids.*, 19:083104.1 – 083104.13, 2007.

[32] E. Lauga and T. R. Powers. The hydrodynamics of swimming microorganisms. *Rep. Prog. Phys.*, 72:096601–096636, 2009.

[33] J. Lighthill. *Mathematical Biofluiddynamics*. Society of Industrial and Applied Mathematics, Philadelphia, 1975.

[34] T. Majmudar, E. E. Keaveny, J. Zhang, and M. J. Shelly. Experiments and the theory of undulatory locomotion in a simple structured medium. *J. R. Soc. Interface*, 9:1809 – 1823, 2012.

[35] E. M. Purcell. Life at low reynolds number. *Am. J. Phys.*, 45:3–11, 1977.

[36] A. J. Reynolds. The swimming of minute organisms. *J. Fluid. Mech.*, 23(2):241 – 260, 1965.

[37] X. N. Shen and P. E. Arratia. Undulatory swimming in viscoelastic fluids. *Phys. Rev. Lett.*, 106:208101.1 – 208101.4, 2011.

[38] S. H. Strogatz. *Nonlinear Dynamics and Chaos*. Perseus Books, Massachusetts, 1994.

[39] S. S. Suares. Unsolved problems in the locomotion of mammalian sperm. In S. Childress, A. Hosoi, W. W. Schultz, and Z. J. Wang, editors, *Natural Locomotion in Fluids*. Springer, New York, 2012.

[40] S. S. Suarez, D. F. Katz, D. H. Owen, J. B. Andrew, and R. L. Powell. Evidence for the function of hyper activated motility in sperm. *Biol. Reprod.*, 44:375–381, 1991.

[41] D. Takagi and N. J. Balmforth. Peristaltic pumping of viscous fluid in an elastic tube. *J. Fluid Mech.*, 672:196–218, 2011.

[42] G. I. Taylor. Analysis of the swimming of microscopic organisms. *Proc. R. Soc. Lond. A*, 209:447–460, 1951.

[43] G. I. Taylor. The action of waving cylindrical tails in propelling microscopic organisms. *Proc. R. Soc. Lond. A*, 211:225–239, 1952.

[44] U. Thiele and E. Knobloch. Driven drops on heterogeneous substrates: onset of sliding motion. *Phys. Rev. Lett.*, 97:204501.1–204501.4, 2006.

[45] S. Yazdi, A. M. Ardekani, and A. Borhan. Locomotion of microorganisms near a no-slip boundary in a viscoelastic fluid. *Phys. Rev. Lett.*, 90:043002.1 – 043002.11, 2014.

Appendix A

Details of Integral Evaluation

When we calculate the exact solution of instantaneous swimming speed for the fixed shape swimmer with $\kappa = 1$, there are six I_n^m integrals evaluation involved. In this appendix, we provide full calculation of these six integrals, which has been omitted in section 2.2.1.

Recall in Chapter Two, the swimmer has a fixed shape $Y = a\cos\xi$ and the washboard wall is defined as $h = b\cos x - 1$. The distance d in between is given as

$$\begin{aligned} d &= a\cos\xi - b\cos x + 1 = a\cos(x+\phi) - b\cos x + 1 \\ &= C_1\cos(x+\Phi) + 1, \end{aligned} \tag{A.1}$$

where $\phi(t)$ measures the phase of translation of the swimmer with respect to the washboard. To sum these two cosine functions, we define $\tan\Phi = \dfrac{\sin\phi}{\cos\phi - \frac{b}{a}}$ and $C_1 = a\sqrt{(\cos\phi - \frac{b}{a})^2 + \sin^2\phi} < 1$.
Now we will calculate six integrals one by one:

$$I_3^0 = \frac{1}{2\pi}\int_0^{2\pi} \frac{1}{(C_1\cos(x+\Phi)+1)^3}\, dx$$

Note: Φ is a phase shift in x. If we integrate over a whole period in x, the phase shift will not change the integration result, i.e.

$$\frac{1}{2\pi}\int_0^{2\pi} \frac{1}{(C_1\cos(x+\Phi)+1)^3}\, dx = \frac{1}{2\pi}\int_0^{2\pi} \frac{1}{(C_1\cos(x)+1)^3}\, dx.$$

Thus,

$$I_3^0 = \frac{1}{2\pi}\int_0^{2\pi} \frac{1}{(C_1\cos(x)+1)^3}\,dx = \frac{1}{2\pi}\cdot\frac{1}{2}\frac{d^2}{d\alpha^2}\left[\frac{1}{\alpha}\int_0^{2\pi}\frac{dx}{1+\frac{C_1}{\alpha}\cos x}\right]\Bigg|_{\alpha=1}.$$

By symmetry, we have

$$\int_0^{2\pi}\frac{dx}{1+\frac{C_1}{\alpha}\cos x} = 2\int_0^{\pi}\frac{dx}{1+\frac{C_1}{\alpha}\cos x}.$$

With a tangent substitution, i.e. $u = \tan\dfrac{x}{2}$, the above integral is changed to be

$$\begin{aligned}\int_0^{\pi}\frac{dx}{1+\frac{C_1}{\alpha}\cos x} &= \int_0^{\infty}\frac{2}{\left(1-\frac{C_1}{\alpha}\right)(1+u^2)+\frac{2C_1}{\alpha}}\,du \\ &= \frac{2}{\left(1+\frac{C_1}{\alpha}\right)\cdot\sqrt{\frac{1-\frac{C_1}{\alpha}}{1+\frac{C_1}{\alpha}}}}\arctan\left(\sqrt{\frac{1-\frac{C_1}{\alpha}}{1+\frac{C_1}{\alpha}}}\cdot u\right)\Bigg|_0^{\infty} \\ &= \frac{\pi}{\sqrt{1-\left(\frac{C_1}{\alpha}\right)^2}}.\end{aligned}$$

Here, we can get

$$I_1^0 = \frac{1}{\sqrt{1-{C_1}^2}} \tag{A.2}$$

and

$$I_3^0 = \frac{1}{2\pi}\cdot\frac{1}{2}\frac{d^2}{d\alpha^2}\left(\frac{2\pi}{\sqrt{\alpha^2-{C_1}^2}}\right)\Bigg|_{\alpha=1} = \frac{1}{2}\cdot\frac{\left(2+{C_1}^2\right)}{\left(1-{C_1}^2\right)^{\frac{5}{2}}}. \tag{A.3}$$

Similarly, we have

$$I_2^0 = -\frac{1}{2\pi}\cdot\frac{d}{d\alpha}\left[\frac{1}{\alpha}\int_0^{2\pi}\frac{dx}{1+\frac{C_1}{\alpha}\cos x}\right]\Bigg|_{\alpha=1} = \frac{1}{\left(1-{C_1}^2\right)^{\frac{3}{2}}}. \tag{A.4}$$

We can separate I_3^1 into two parts as

$$I_3^1 = \frac{1}{2\pi}\left(\int_0^{2\pi} \frac{1}{(Y-h)^2}\, dx + \int_0^{2\pi} \frac{h}{(Y-h)^3}\, dx\right),$$

and calculate these two parts one by one. We have found out earlier that

$$\frac{1}{2\pi}\int_0^{2\pi} \frac{1}{(Y-h)^2}\, dx = \frac{1}{\left(1-{C_1}^2\right)^{\frac{3}{2}}}.$$

Notice that

$$\frac{1}{2\pi}\int_0^{2\pi} \frac{h}{(Y-h)^3}\, dx = \frac{1}{2\pi}\int_0^{2\pi} \frac{b\cos x}{(C_1\cos(x+\Phi)+1)^3}\, dx - I_3^0,$$

and

$$\begin{aligned}&\int_0^{2\pi} \frac{b\cos x}{(C_1\cos(x+\Phi)+1)^3}\, dx \\ &= b\cos\Phi\int_0^{2\pi} \frac{\cos\bar{x}}{(C_1\cos\bar{x}+1)^3}\, d\bar{x} + b\sin\Phi\int_0^{2\pi} \frac{\sin\bar{x}}{(C_1\cos\bar{x}+1)^3}\, d\bar{x}.\end{aligned}$$

Due to the 2π-periodic condition on $\cos\bar{x}$, we have

$$b\sin\Phi\int_0^{2\pi} \frac{\sin\bar{x}}{(C_1\cos\bar{x}+1)^3}\, d\bar{x} = 0.$$

Thus, we only need to deal with the first integral.
Notice that

$$\int_0^{2\pi} \frac{\cos\tilde{x}}{(A\cos\tilde{x}+1)^3}\, d\tilde{x} = \frac{1}{2}\frac{d^2}{d\alpha^2}\left[\frac{1}{\alpha}\int_0^{2\pi} \frac{\cos\tilde{x}}{1+\frac{A}{\alpha}\cos\tilde{x}}\, d\tilde{x}\right]\Bigg|_{\alpha=1}.$$

Again, we can use a tangent substitution as what we did for I_3^0 and get

$$b\cos\Phi\int_0^{2\pi} \frac{\cos\bar{x}}{(C_1\cos\bar{x}+1)^3}\, d\bar{x} = b\cos\Phi\left(-\frac{3C_1\pi}{\left(1-{C_1}^2\right)^{\frac{5}{2}}}\right).$$

Thus,

$$I_3^1 = \frac{1}{2\pi}\left(\frac{2\pi}{\left(1-{C_1}^2\right)^{\frac{3}{2}}} + b\cos\Phi\left(-\frac{3C_1\pi}{\left(1-{C_1}^2\right)^{\frac{5}{2}}}\right) - \frac{\pi\left(2+{C_1}^2\right)}{\left(1-{C_1}^2\right)^{\frac{5}{2}}}\right). \quad \text{(A.5)}$$

Similarly,

$$I_2^1 = \frac{1}{2\pi}\left(\int_0^{2\pi}\frac{1}{Y-h}\,dx + \int_0^{2\pi}\frac{h}{(Y-h)^2}\,dx\right) = I_1^0 + \frac{1}{2\pi}\int_0^{2\pi}\frac{h}{(Y-h)^2}\,dx.$$

Again,

$$\frac{1}{2\pi}\int_0^{2\pi}\frac{h}{(Y-h)^2}\,dx = \frac{1}{2\pi}\int_0^{2\pi}\frac{b\cos x}{(C_1\cos(x+\Phi)+1)^2}\,dx - I_2^0,$$

and

$$\begin{aligned}
&\int_0^{2\pi}\frac{b\cos x}{(C_1\cos(x+\Phi)+1)^2}\,dx\\
=&b\cos\Phi\int_0^{2\pi}\frac{\cos\tilde{x}}{(C_1\cos\tilde{x}+1)^2}\,d\tilde{x} + b\sin\Phi\int_0^{2\pi}\frac{\sin\tilde{x}}{(C_1\cos\tilde{x}+1)^2}\,d\tilde{x}\\
=&b\cos\Phi\left[-\frac{d}{d\alpha}\left(\frac{1}{\alpha}\int_0^{2\pi}\frac{\cos\tilde{x}}{1+\frac{C_1}{\alpha}\cos\tilde{x}}\,d\tilde{x}\right)\right]\Bigg|_{\alpha=1} = -\frac{2\pi(C_1 b\cos\Phi+1)}{\left(1-{C_1}^2\right)^{\frac{3}{2}}}.
\end{aligned}$$

Thus, combing all the parts, we get

$$I_2^1 = -\frac{C_1(C_1+b\cos\Phi)}{\left(1-{C_1}^2\right)^{\frac{3}{2}}}. \quad \text{(A.6)}$$

The very last integral we need to deal with is I_3^2, which again can be separated into two parts as

$$\begin{aligned}
I_3^2 &= \frac{1}{2\pi}\left(\int_0^{2\pi}\frac{Y+h}{(Y-h)^2}\,dx + \int_0^{2\pi}\frac{h^2}{(Y-h)^3}\,dx\right)\\
&= \frac{1}{2\pi}\left(-\frac{2\pi({C_1}^2+2C_1 b\cos\Phi+1)}{\left(1-{C_1}^2\right)^{\frac{3}{2}}} + \int_0^{2\pi}\frac{h^2}{(Y-h)^3}\,dx\right).
\end{aligned}$$

The second integral could be separated into three more parts as

$$\int_0^{2\pi} \frac{h^2}{(Y-h)^3}\, dx = \int_0^{2\pi} \frac{b^2\cos^2(\bar{x}-\Phi)}{(C_1\cos\bar{x}+1)^3}\, d\bar{x} + \frac{6C_1\pi b\cos\Phi}{\left(1-{C_1}^2\right)^{\frac{5}{2}}} + \frac{\pi(2+{C_1}^2)}{\left(1-{C_1}^2\right)^{\frac{5}{2}}}.$$

The first integral on the right hand side of above equation could be evaluated by tangent substitution again, and we get

$$\int_0^{2\pi} \frac{b^2\cos^2(\bar{x}-\Phi)}{(C_1\cos\bar{x}+1)^3}\, d\bar{x} = b^2\cos^2\Phi\pi\left(\frac{1+2{C_1}^2}{\left(1-{C_1}^2\right)^{\frac{5}{2}}}\right) + b^2\sin^2\frac{\pi}{\left(1-{C_1}^2\right)^{\frac{3}{2}}}.$$

Combing all the parts, it gives

$$\begin{aligned} I_3^2 =& \frac{1}{2\pi}\Bigg[-\frac{2\pi({C_1}^2+2C_1b\cos\Phi+1)}{\left(1-{C_1}^2\right)^{\frac{3}{2}}} + b^2\cos^2\Phi\pi\left(\frac{1+2{C_1}^2}{\left(1-{C_1}^2\right)^{\frac{5}{2}}}\right) \\ &+ b^2\sin^2\frac{\pi}{\left(1-{C_1}^2\right)^{\frac{3}{2}}} - 2\left(-\frac{3C_1\pi b\cos\Phi}{\left(1-{C_1}^2\right)^{\frac{5}{2}}}\right) + \frac{\pi(2+{C_1}^2)}{\left(1-{C_1}^2\right)^{\frac{5}{2}}}\Bigg], \end{aligned} \tag{A.7}$$

where

$$\sin\Phi = \frac{\sin\phi}{\sqrt{\sin^2\phi + \left(\cos\phi - \frac{b}{a}\right)^2}} \quad \text{and} \quad \cos\Phi = \frac{\cos\phi - \frac{b}{a}}{\sqrt{\sin^2\phi + \left(\cos\phi - \frac{b}{a}\right)^2}}.$$

Hence, all six integrals we need for evaluating instantaneous swimming speed are solved and their solutions are listed as (A.2)-(A.7).